ChemCatChem

Research Article
doi.org/10.1002/cctc.202401702

Chemistry Europe
European Chemical Societies Publishing

www.chemcatchem.org

Gold Nanoparticle-Catalyzed Solvent Switchable Selective Partial Reduction of Nitrobenzene to *N*-Phenylhydroxylamine and Azoxybenzene

Simon Doherty,*[a] Julian G. Knight,*[a] Hussam Y. Alharbi,[a, b] Reece Paterson,[a] Corinne Wills,[a] Casey Dixon,[a] Thomas W. Chamberlain,*[c] Han Yan,[c] Anthony Griffiths,[c] Helen Daly,[d] Sarayute Chansai,[d] and Christopher Hardacre[d]

This article is dedicated to the memory of Professor Stephen A. Westcott, a great ambassador for chemistry in Canada and across the globe and the best and most sincere of friends, who is greatly missed.

Impregnation of phosphine-decorated polymer-immobilized ionic liquid with the tetrachloroaurate anion results in reduction of the gold(III) to gold(I) with concomitant oxidation of the phosphine to its oxide. In situ reduction of the resulting precursor, AuCl@O = PPh_2-PEGPIILS, generated the corresponding O = PPh_2-PEGPIIL-stabilized AuNPs, AuNP@O = PPh_2-PEGPIILS, which is a highly active and selective catalyst for the solvent-dependent partial reduction of nitrobenzene to *N*-phenylhydroxylamine in water and azoxybenzene in ethanol. The initial TOFs are comparable to those obtained with gold nanoparticles generated by reduction of tetrachloroaurate-impregnated phosphine oxide-decorated polymer-immobilized ionic liquid $AuCl_4$@O = PPh_2-PEGPIILS, i.e., the activity and selectivity profiles do not appear to depend on whether the AuNPs are generated from Au(III) or in situ-generated Au(I). In stark contrast, gold nanoparticles prepared by $NaBH_4$ reduction of AuCl@PPh_2-PEGPIILS based on gold(I) confined in phosphine-modified polymer-immobilized ionic liquid gave markedly lower initial TOFs. The use of dimethylamine borane (DMAB) as the hydrogen donor resulted in a substantial and dramatic enhancement in activity for reductions conducted in water compared with $NaBH_4$ and the initial TOF of 20,400 mol nitrobenzene converted mol Au^{-1} h^{-1} obtained with AuNPs generated in situ from $AuCl_4$@O = PPh_2-PEGPIILS is among the highest to be reported for the metal nanoparticle catalyzed selective reduction of nitrobenzene to *N*-phenylhydroxylamine; this is a significant improvement on existing protocols, which should enable the partial selective reduction of nitroarenes to be conducted in water with a low catalyst loading under extremely mild conditions.

1. Introduction

N-Arylhydroxylamines are important intermediates for the synthesis of bioactive molecules such as acetaminophen and pyraclostrobin, bioactive derivatives of antibiotics[1–11] and fine chemicals,[12–14] as well as polymerization inhibitors[15,16] and reagents in organic synthesis.[17–23] While this motif has been prepared by the catalytic *N*-arylation of the parent hydroxylamines[24–27] as well as the selective reduction of aldoximes,[28–33] the selective partial reduction of nitro aromatic compounds either under an atmosphere of hydrogen or with a hydrogen donor has been more widely developed, as it is an operationally more convenient and versatile protocol.[34–53] However, the selective partial reduction of nitroarenes is extremely difficult to achieve, as over-reduction to the thermodynamically favored aryl amine must be prevented and the factors that control this selectivity are still poorly understood. To this end, common protocols involve stoichiometric reductions with zinc, tin, antimony, or bismuth[15,33–38] as well as catalytic reductions using either heterogeneous or nanoparticle-based systems such as Rh/C,[39,40] Pt/SiO_2,[41] RuNP/CNT,[42] RuNPs supported on polystyrene,[43] PtNPs immobilized on Amberlite IRA 900 resin,[44] c-PtN/C,[45] polystyrene-supported IrNPs,[46]

[a] Dr. S. Doherty, Dr. J. G. Knight, Dr. H. Y. Alharbi, R. Paterson, Dr. C. Wills, Dr. C. Dixon
Newcastle University Centre for Catalysis (NUCAT), School of Chemistry, Newcastle University, Bedson Building, Newcastle upon Tyne NE1 7RU, UK
E-mail: simon.doherty@ncl.ac.uk
julian.knight@ncl.ac.uk

[b] Dr. H. Y. Alharbi
Chemistry Department, Faculty of Science, Taibah University, Yanbu 46423, Saudi Arabia

[c] Prof. T. W. Chamberlain, H. Yan, Dr. A. Griffiths
Institute of Process Research & Development School of Chemistry, University of Leeds, Woodhouse Lane, Leeds LS2 9JT, UK
E-mail: t.w.chamberlain@leeds.ac.uk

[d] Dr. H. Daly, Dr. S. Chansai, Prof. C. Hardacre
School of Chemical Engineering and Analytical Sciences, The University of Manchester, The Mill, Sackville Street Campus, Manchester M13 9LP, UK

Supporting information for this article is available on the WWW under https://doi.org/10.1002/cctc.202401702

solid-supported PtNPs deactivated with an amine,[47,48] silica-supported PdNPs,[49] and palladium nanoclusters.[50] However, many of these approaches experience detrimental drawbacks, such as the use of either large quantities of costly noble metal-based catalysts or stoichiometric quantities of earth abundant metal reagents, the need for an additive, low yields, poor selectivity profiles, low functional group tolerance, slow rates, the need for forcing conditions, and negative environmental credentials due to the use of toxic or hazardous reagents as well as the generation of stoichiometric quantities of by-products.

Interestingly, several nanoparticle-based catalysts have been reported to give good yields and high selectivities for the partial reduction of nitrobenzene to *N*-phenylhydroxylamine under mild conditions; moreover, these systems have improved our understanding of what factors influence selectivity and thereby will inform the design of more efficient catalysts. For instance, ultrathin platinum nanowires modified with ethylenediamine[51] and NanoSelect nanoparticulate platinum supported on activated carbon in the presence of a small amount of *N,N,N′,N′*-tetramethylethylenediamine[45] both catalyze the reduction of nitrobenzene to afford *N*-phenylhydroxylamine with >97% selectivity. The high selectivity obtained with the former system was attributed to coordination of the σ-donor amine rendering the surface of the nanoparticle electron-rich which favored binding of the electron-deficient substrate over the electron-rich hydroxylamine,[51] while the latter was attributed to facile substitution of the *N*-phenylhydroxylamine from the surface of the nanoparticle by the amine additive.[45] High selectivity for the partial reduction of nitrobenzene to *N*-phenylhydroxylamine with ultra-small PdNPs supported on perfluoroalkyl-modified cellulose was also attributed to preferential adsorption of the nitrobenzene over *N*-phenylhydroxylamine on the hydrophobic surface of the catalyst as well as its electron-rich structure.[52] Similarly, solid-supported platinum(0) nanoparticles catalyze the selective partial reduction of nitroarenes to *N*-arylhydroxylamines with hydrazine hydrate in PEG-400; in this system the PEG was proposed to form a hydrogen bond with the *N*-arylhydroxylamine which prevented further reduction by assisting its removal from the surface.[44] In addition to these examples, there are numerous related reports in which the activity and/or selectivity of a metal nanoparticle-based catalyst has been improved in the presence of a σ-donor ligand or an organic modifier which act by modulating the surface electronic structure of the catalyst and/or its steric environment, controlling the solubility of the reactants through the hydrophobic/hydrophilic environment at the catalyst surface[53–57] or by tuning metal-support interactions.[58,59] While phosphine donors have been widely used to enhance the performance of Ru, Pd, Au, Pt, and Rh nanoparticles as catalysts for hydrogenative transformations,[60–72] amine additives and amine-modified supports have also been reported to improve the performance of NP-based catalysts; in most cases this enhancement has been attributed to either the formation of ultra-small, highly dispersed nanoparticles, the high surface electron density arising from coordination of the amine to the NP surface, or a cooperative role assisting the elementary steps of the catalytic cycle.[45,51,66,73–89]

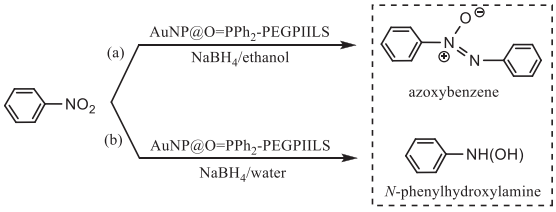

Scheme 1. Selective partial reduction of nitrobenzene with AuNP@O = PPh_2-PEGPIILS. (a) Reaction conducted in ethanol and catalyzed by AuNP@O = PPh_2-PEGPIILS to afford azoxybenzene and (b) reaction conducted in water and catalyzed by AuNP@ O = PPh_2-PEGPIILS to afford *N*-phenylhydroxylamine.

Embracing this concept, we have been exploring the use of heteroatom donor (HAD)-modified polymer-immobilized ionic liquids (PIILs) as supports for the stabilization of metal nanoparticles on the basis that the ionic liquid component would provide stabilization through weak electrostatic interactions to the surface of the NP[102] while coordination of the heteroatom donor to the surface would supplement this stabilization and thereby prevent aggregation to less active species as well as assist impregnation of the precursor onto the support through metal–ligand coordination, which could control the growth and dispersion of the nanoparticles.[103–112] Moreover, the escalating number of examples of ligand-enhanced performance for NP-based catalysts suggests that HAD-modified PIILs could be versatile supports for modulating the properties of NP, as the nature of the heteroatom donor and its concentration or loading, the ionic micromovement, the porosity, and the surface hydrophilicity can be systematically modified to improve and optimize catalyst performance and identify new applications and processes.[113,114]

One of our early studies reported that AuNPs stabilized by a phosphine-decorated polymer-immobilized ionic liquid was an efficient, solvent-dependent selective catalyst for the partial reduction of nitrobenzene to *N*-phenylhydroxylamine or azoxybenzene (Scheme 1a,b).[106] While our initial premise was to investigate whether the phosphine donor would influence the efficiency of the catalyst either by modifying the surface electronic structure and steric environment and/or controlling the size and morphology of the NPs. Subsequent studies have revealed that the AuNPs were in fact supported by a phosphine oxide-decorated polymer-immobilized ionic liquid. The phosphine oxide appeared to result from a facile redox reaction between the phosphine-decorated PIIL and the tetrachloroaurate anion during impregnation of the polymer, in much the same manner as phosphines reduce palladium acetate to active palladium(0) phosphine-based species.[115] As a result of this serendipitous discovery, we attempted to undertake a comparison of the performance of AuNPs stabilized by a phosphine oxide-decorated PIIL with those stabilized by the corresponding phosphine-decorated polymer to establish whether the heteroatom influences catalyst efficacy, i.e., a good σ-donor versus a hemilabile phosphine oxide. Herein we report the results of this preliminary comparison, which has shown that AuNPs generated by reduction of Au(I)-impregnated phosphine oxide-decorated PIIL, derived from the redox reaction between $[AuCl_4]^-$ and

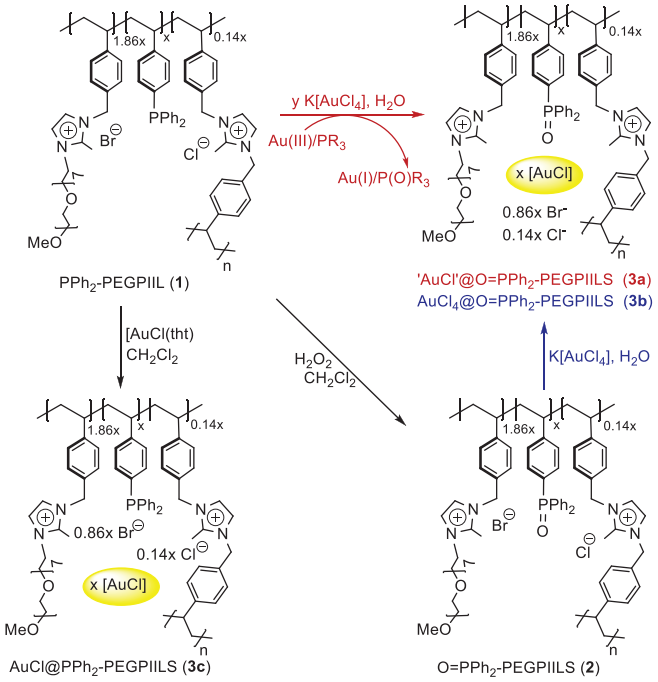

Scheme 2. Composition of PPh_2-PEG-PIIL (**1**) and O = PPh_2-PEGPIIL (**2**) and synthesis and composition of gold(I) and gold(III)-impregnated O = PPh_2-PEGPIIL, **3a** and **3b**, respectively, and gold(I)Cl-impregnated PPh_2-PEGPIIL (**3c**). The corresponding PIIL-stabilized gold nanoparticles **4a–c** were generated from **3a–c** using either $NaBH_4$ or NMe_2HBH_3 as the reducing agent, as specified in the discussion.

PIIL-anchored phosphine, or by reduction of $[AuCl_4]^-$ impregnated in pre-formed phosphine oxide-decorated PIIL have very similar activity and selectivity profiles for the partial reduction of nitrobenzene. In contrast, AuNPs generated from Au(I)-impregnated phosphine-decorated polymer-immobilized ionic liquid are markedly less active as a catalyst for the partial and complete reduction of nitrobenzene than their phosphine oxide-based counterpart. In addition, a subsequent survey of the catalyst efficacy as a function of the hydrogen donor revealed that reductions conducted in water using DMAB as the hydrogen source are significantly faster than those with $NaBH_4$.The initial TOF of 20,400 h^{-1} is in fact amongst the highest to be reported for the selective partial reduction of nitrobenzene to *N*-phenylhydroxylamine with a nanoparticle-based catalyst. This is a distinct improvement on existing protocols, many of which require an organic solvent to achieve high selectivity or a large excess of reducing agent, a high reaction temperature, or a high catalyst loading.

2. Results and Discussion

2.1. Synthesis and Characterization of Precatalysts (3a–c) and Catalysts (4a–c)

The composition of the phosphine and phosphine oxide-decorated polymer-immobilized ionic liquids, **1** and **2**, respectively, and the Au(I) or Au(III)-loaded precursors used in this study are shown in Scheme 2. Polymer **1** was prepared by the AIBN-initiated radical polymerization of 4-diphenylphosphinostyrene, imidazolium-based monomer, and an appropriate amount of cross-linker to afford polymer with a phosphine to total imidazolium ratio of 1:2 while **2** was generated by hydrogen peroxide-mediated oxidation of **1**[104] and isolated in near quantitative yield as a free-flowing white powder. The composition and purity of **1** and **2** were confirmed by a combination of ^1H, ^{31}P and ^{13}C NMR spectroscopy (Figures S3–S5 and S9–S11). Impregnation of **1** by exchange of half of the halide anions for $[AuCl_4]^-$ resulted in rapid reduction of the Au(III) to Au(I) ($E_{1/2}$ = +1.36 V) with concomitant oxidation of the phosphine to its oxide ($E_{1/2}$ = +1.0 V)[116] to afford the gold(I)-based phosphine oxide-decorated polymer-immobilized ionic liquid AuCl@O = PPh_2-PEGPIILS (**3a**), while the corresponding gold(III)-loaded phosphine oxide-decorated polymer-immobilized ionic liquid, $AuCl_4$@O = PPh_2-PEGPIILS (**3b**) was prepared by impregnation of phosphine oxide-decorated polymer-immobilized ionic liquid **2** with $[AuCl_4]^-$; in both cases a gold to phosphine oxide stoichiometry of 1:1 was targeted. Finally, (THT)AuCl was identified as a suitable precursor to prepare AuCl@PPh_2-PEGPIILS (**3c**) which could be reduced to afford AuNPs-stabilized by PPh_2-PEGPIIL (**1**) as Au(I) is not capable of oxidizing the phosphine;[117] however, it could form a Au–P interaction and thereby assist impregnation, influence nanoparticle growth and dispersion and/or supplement the weak stabilization of the NPs by the ionic polymer. Full characterization of precursors **3a–c** has been provided in the Supporting Information. As our preliminary studies on this project demonstrated that gold nanoparticles generated in situ by reduction of the corresponding tetrachloroaurate-loaded precursor are as efficient as their ex situ-generated counterparts for the reduction of nitroarenes, **3a–c** were used for comparative catalyst evaluation while samples of **4a–c** were generated under conditions of catalysis to obtain TEM and XPS characterization data on the active species. Generation of the catalyst in situ immediately prior to its use offers several practical advantages as the precursor can be stored indefinitely and handled without any special precautions and it also enables different catalyst generation protocols to be explored to facilitate rapid throughput catalyst and reaction screening. The gold loadings of precatalysts **3a–c** were determined to be between 0.41 and 0.45 mmol g^{-1}, using ICP-OES. The solid state ^{31}P NMR spectrum of **3a** contained two broad signals one at δ 25.1 ppm associated with the phosphine oxide and the other at δ 32.1 ppm which is consistent with a Au—PPh_2-PEGPIILS interaction (vide infra) while the solid state ^{31}P NMR spectrum of **3b** contained a single broad resonance at δ 27.1 ppm as this precatalyst was prepared by impregnation of phosphine oxide-decorated polymer **2** with tetrachloroaurate (Figures S11 and S16). In contrast, the solid state ^{31}P NMR spectrum of **3c** contained a major resonance at δ 32 ppm, which is consistent with an Au—P interaction as the ^{31}P signal for PPh_2-PEGPIIL appeared at ca. δ -6 ppm and the magnitude of this complexation shift is similar to that reported for $(Ph_3P)AuCl$, which appears at δ 33.15 ppm.[118,119] The minor shoulder at δ 27 ppm (<5%) is associated with a small amount of oxide O = PPh_2-PEGPIIL which was present in the polymer prior to impregnation (Figure S21). The presence of a strong P=O stretching band at 1174 cm^{-1} in the IR spectrum of **3a** supports the pres-

ence of oxide and the small red shift of this band with respect to 1181 cm^{-1} for the corresponding P=O stretch in **2** could be indicative of a weak Au—O = PPh_3 interaction (Figure S19). The ^{13}C CP MAS NMR spectra of **3a** and **3b** contain a series of signals in the region of δ 121–111 ppm associated with the imidazolium ring and the aromatic carbon atoms of the polystyrene as well as a set of signals at higher field between δ 11 and 52 ppm assigned to the methyl and methylene groups attached to the nitrogen atoms of the imidazolium ring and an intense signal at δ 70 and a weaker one at δ 59 ppm associated with the methylene carbon atoms on the PEG and the terminal methoxy, respectively.

Surface characterization of the gold(I) and gold(III)-loaded precursors **3a–c** was undertaken by X-ray photoelectron spectroscopy with the P 2p and Au 4f regions analyzed. The 2p region for polymer **1** contained two $2p_{3/2}$ peaks one at 130.6 eV associated with PPh_2-PEGPIIL and the other at 132.2 eV, which is consistent with P(V) in O = PPh_2-PEGPIIL (**2**) resulting from surface oxidation;[120a–c] this assignment has been supported by analyzing a sample of freshly prepared **2** generated by hydrogen peroxide-mediated oxidation of **1** (Figure S8) There was no significant shift in the binding energies of the 2p doublet for **2** upon impregnation with the $[AuCl_4]^-$ anion, whereas impregnation of **1** with $[AuCl_4]^-$ resulted in a shift of the $2p_{3/2}$ peak from 130.2 eV to higher binding energy commensurate with oxidation of the phosphine to its oxide.[120a] Impregnation of **1** with (THT)AuCl resulted in the complete disappearance of the $2p_{3/2}$ peak at 130.2 eV which we tentatively suggest to be due to formation of a Au–PPh_2-PEGPIIL interaction with transfer of electron density from the phosphorus to the surface of the gold nanoparticle as this would shift the $2p_{3/2}$ peak to higher binding energy such that it becomes coincident with that for O = PPh_2-PEGPIIL. Analysis of the gold 4f core level of **3a** revealed a major $4f_{7/2}$ peak at 84.7 eV which is in the region for a Au(I)-Cl species and consistent with reduction of the $[AuCl_4]^-$ anion by the phosphine during impregnation (Figure S13).[120d–f] For comparison, the 4f region for **3b** contained two distinct $4f_{7/2}$ peaks; one with a binding energy of 87.0 eV, which corresponds to a Au(III) species,[120g–m] while the second peak with a binding energy of 84.5 eV is most likely associated with monovalent gold chloride generated by reduction of Au(III) under the XPS beam (Figure S18). The 4f region of precatalyst **3c** contained a major $4f_{7/2}$ peak with a binding energy of 85.5 eV, which belongs to a Au(I) species together with a minor component with slightly lower binding energy of 84.6 eV, which we tentatively assign to the Au–P interaction identified above in the P 2p region as donation from the phosphine to the gold would render the Au(I) more electron-rich (Figure S23).

Surface characterization of catalysts **4a–c** generated in situ by reduction of **3a–c** with either $NaBH_4$ or NMe_2HBH_3 was also undertaken. Catalysts generated by reduction with $NaBH_4$ all contained two Au $4f_{7/2}$ peaks, a major component attributed to Au(0) species with a binding energy of 83.4 eV[120g–m] and a minor component at 84.5 eV, which most likely corresponds to monovalent gold species (Figure 1a–c).[120d–f] Similarly, catalysts generated by reduction with DMAB also contained two pairs of doublets in the 4f region, although under these conditions there was significantly more of the Au(I) species and, in some cases, it was the major component (Figure 1d–f). As the relative ratios of these doublets varied as a function of the precatalyst and the reducing agent, quantitative analysis of the 4f components was used to determine the proportions of Au(0) and Au(I) species (Table S12). Interestingly, for each precatalyst **3a–c** less reduction to Au(0) occurs after treatment with DMAB compared with $NaBH_4$, which may be associated with the power of $NaBH_4$ as a reducing agent compared with DMAB or easier access of the charged borohydride to the tetrachloropalladate impregnated in the polymer-immobilized ionic liquid compared with DMAB, which is neutral. This difference is most evident for the nanoparticles generated by sodium borohydride-mediated reduction of **3a** which gave ca. 13 at.% Au(I) and 87 at.% Au(0) while the corresponding reduction with DMAB gave a much lower conversion to Au(0) such that Au(I) was the major species with 64 at.% Au(I) and 36 at.% Au(0). Similarly, the reduction of **3b** with $NaBH_4$ gave 83 at.% Au(0) compared with 70 at.% for DMAB. In contrast, while the reduction of **3c** with DMAB only gave 47 at.% Au(0), its reduction with $NaBH_4$ only gave 66 at.% Au(0) which is lower than the 87 and 83 at.% for **3a** and **3b,** respectively, under the same conditions. This reluctance of **3c** toward reduction with $NaBH_4$ may be indicative of Au species coordinated to a Lewis basic phosphine that would limit their reducibility whereas **3a** and **4b** both contain phosphine oxide-decorated PIIL, which acts as a hemilabile ligand and is less likely to coordinate to the Au(I) or Au(III).

TEM micrographs of **4a–c**, generated from **3a–c** by in situ reduction with $NaBH_4$, revealed that the gold nanoparticles are near monodisperse and that the average diameter of 1.7 ± 0.5 nm for **4c**, generated from gold(I) impregnated in PPh_2-PEGPIILS, is slightly smaller than either **4a** or **4b**, generated from Au(I) (2.9 ± 0.9 nm) or Au(III) (2.1 ± 0.7 nm) immobilized by phosphine oxide-decorated O = PPh_2-PEGPIILS; representative micrographs and distribution histograms based on >100 particles are shown in Figure 2 and Figures S24, S28, and S32 in the Supporting Information. For comparison, AuNPs stabilized by nona-PEG-branched triazole dendrimers, PEG-substituted tris-1,2,3-triazoles and dendritic triazoles all have diameters close to 3 nm,[121a–c] gold NPs embedded in imidazolium-based organic polymers are ultrafine and have average diameters of 1.8 nm,[122] while AuNP-polymeric ionic liquid nanocomposites have slightly larger mean diameters of 4.0–4.5 nm[123a] as do those immobilized on ionic liquid hybrid γ-Al_2O_3 with average diameters of 6.5–6.7 nm,[124] C_4,C_n-imidazolium-based ILs (n = 12–14) with average diameters of 5.9 nm,[125] and supported ionic liquid-like phases, which have diameters up to 23 nm.[123b]

Having established that impregnation of **1** with K[$AuCl_4$] resulted in oxidation of the phosphine and reduction of Au(III) to Au(I), the reaction between K[$AuCl_4$] and triphenylphosphine was monitored as a model to map the progress of the reaction and identify intermediates and products as a function of time. To this end, an NMR tube was charged with a solution of K[$AuCl_4$] in dry ethanol and a solution of PPh_3 in dry dichloromethane in a glove box to exclude air and the reaction monitored by recording ^{31}P NMR spectra at 10-min intervals across 18 h; representative spectra at selective time intervals are shown as a stacked plot in Figure 3b and the entire set of spectra are presented in Figure S1 of the Supporting Information. The associated composition time profile in Figure 3a shows that the

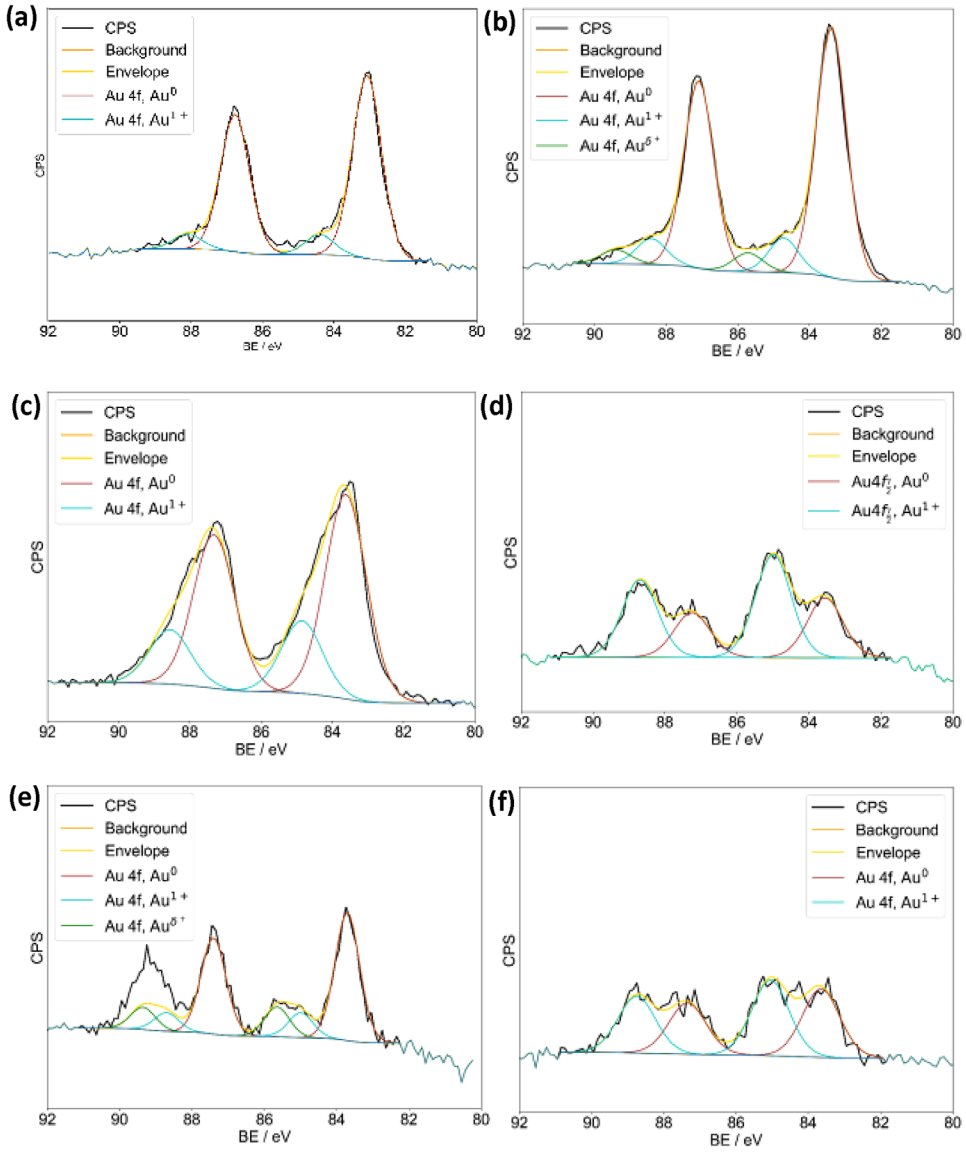

Figure 1. (a–c) Au 4f core level XPS spectra of **4a–c**, respectively, generated by $NaBH_4$-mediated reduction of **3a–c**, and (d–f) Au 4f core level XPS spectra of **4a–c**, respectively, generated by DMAB-mediated reduction of **3a–c**.

$K[AuCl_4]$ is rapidly reduced to Au(I) as evidenced by the instantaneous appearance of a signal at δ 33 ppm corresponding to $(Ph_3P)AuCl$, the identity of which was confirmed by preparing an authentic sample from the reaction between (THT)AuCl and PPh_3.[118,119] The formation of $(Ph_3P)AuCl$ was accompanied by the instantaneous appearance of a low field signal at δ 62 ppm, identified as PPh_3Cl_2 by comparison of the chemical shift with an authentic sample purchased from a commercial supplier; this was slowly consumed over time to afford $O=PPh_3$. ^{31}P NMR analysis of the same reaction conducted on a larger scale to isolate and identify the intermediate and products also showed a very minor but measurable amount of an additional species at δ 44 ppm; this chemical shift is consistent with that reported for $(Ph_3P)AuCl_3$ and its identity was confirmed by preparing a sample by oxidation of $(Ph_3P)AuCl$ with chlorine.

Thus, the reaction between triphenylphosphine and $K[AuCl_4]$, and thereby the impregnation of **1** with $K[AuCl_4]$, results in a redox reaction involving reduction of Au(III) to Au(I) with concomitant oxidation of the triphenylphosphine to PPh_3Cl_2 followed by a subsequent slow hydrolysis to its oxide. At this stage there is still a question about the origin of the oxygen for the $O=PPh_3$, which could be due to either a small amount of adventitious water in the ethanol, or ethanol itself, the latter would require the concomitant formation of either chloroethane or diethyl ether. To this end, we have considered several possible mechanisms for the formation of the $O=PPh_3$ and the Au(I) species involving water and ethanol as shown in Figure 4. In the case of water as the nucleophile, the reaction would be initiated by attack at the activated gold(III)-coordinated phosphine and liberation of HCl prior to the redox step that resembles the phosphine-mediated reduction of Pd(II) to Pd(0) (pathway a),[115] whereas the ethanol-mediated pathway would involve oxidation of the phosphine in the first step to liberate the phosphonium salt $[PPh_3Cl]^+[Cl]^-$, nucle-

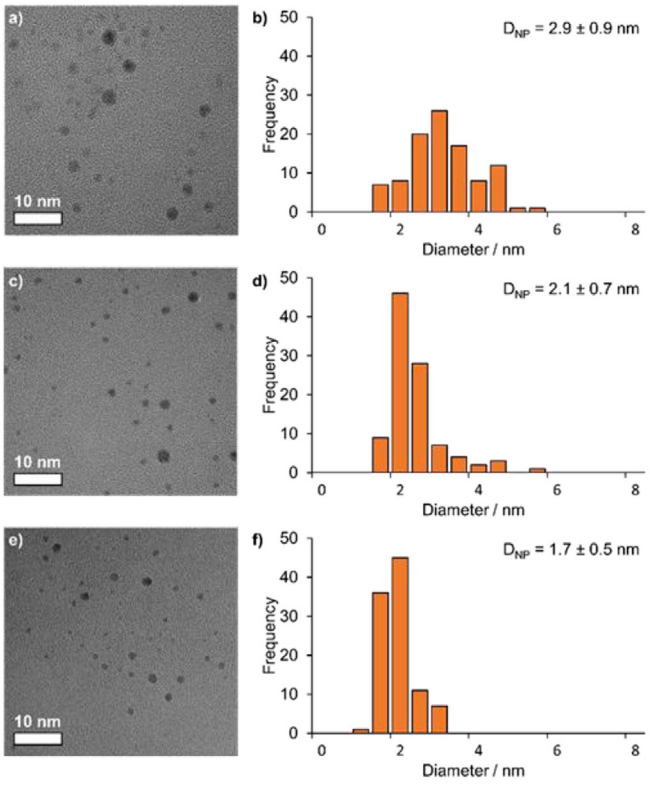

Figure 2. (a, c, and e) HRTEM images of **4a–c**, respectively, generated by in situ reduction of **3a–c** with $NaBH_4$, and (b, d, and f) corresponding size distribution determined by counting >100 particles. Mean particle diameters are 2.9 ± 0.9, 2.1 ± 0.7, and 1.7 ± 0.5 nm for **4a**, **4b**, and **4c**, respectively. Scale bars are 10 nm (white).

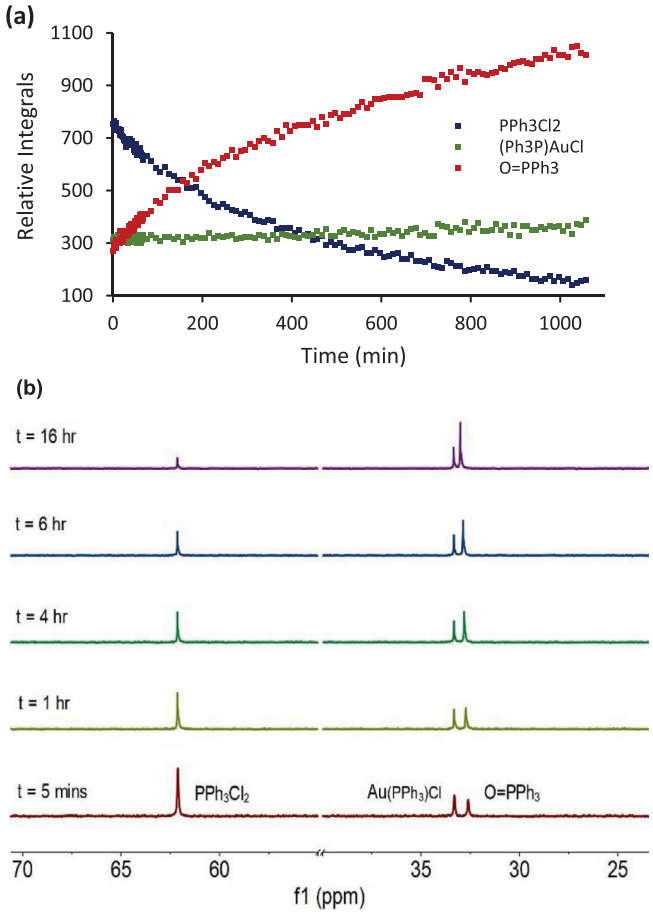

Figure 3. (a) Composition time profile for the stoichiometric reaction between $K[AuCl_4]$ and PPh_3 conducted under nitrogen in a mixture of ethanol and dichloromethane at 25 °C and (b) representative stacked plot of the ^{31}P NMR spectra recorded at selected times showing the progress of the reaction as a function of time.

ophilic displacement of the chloride by ethanol followed by an S_N2 reaction with the chloride to liberate chloroethane and O = PPh_3 in a sequence resembling the Appel reaction (pathway b).[126] Alternatively, the gold-coordinated phosphine may be activated toward nucleophilic attack by chloride to afford the $[(Ph_3ClP)AuCl_3]^-$ anion which could then undergo P—Cl bond-forming reductive elimination to liberate the Ph_3PCl_2 identified in the early stages of the reaction (pathway c) or the phosphonium salt $[PPh_3Cl]^+[Cl]^-$ could be generated by direct P—Cl bond-forming reductive elimination from $(Ph_3P)AuCl_3$ in much the same manner as that reported by Toste and Winston for the facile P—C-based reductive elimination at gold(III).[127] At this stage, we tentatively favor either pathway b or c as both account for the formation of the PPh_3Cl_2 or $[PPh_3Cl][Cl]$ identified by ^{31}P NMR spectroscopy as an intermediate in the redox transformation. While hindsight suggests that this redox process

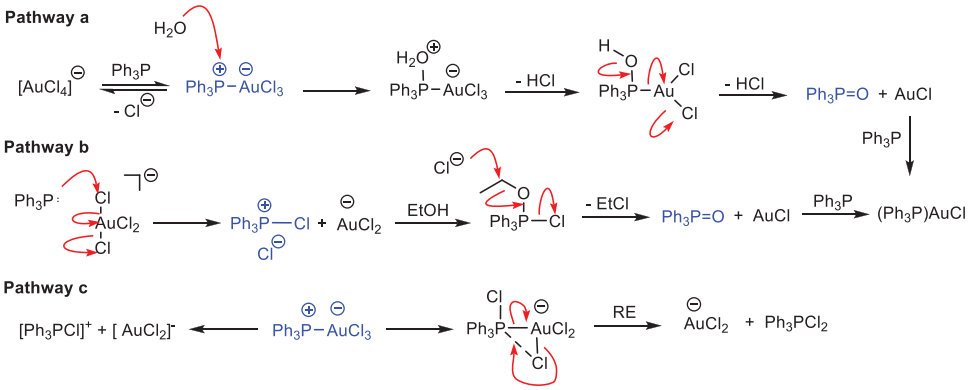

Figure 4. Possible pathways for the phosphine-mediated reduction of Au(III) to Au(I) with formation of triphenylphosphine oxide: (a) water-mediated, (b) ethanol-mediated, and (c) P-Cl bond-forming reductive elimination.

should have been anticipated at the inception of this project during the catalyst design, it is worth noting that there appear to be some related examples of unexpected, serendipitous oxidation of phosphine-modified supports during the preparation of metal nanoparticles. For example, microenvironment-engineered RuNPs incorporated into a phosphine-modified silica nanoreactor[72] and RuNPs stabilized by phosphine-rich cross-linked network polymers[128] are both likely to be the corresponding phosphine oxide-supported RuNPs as impregnation of the support with ruthenium trichloride would result in reduction of Ru(III) to Ru(II) with concomitant oxidation of the phosphine.

As the oxidation of $(Ph_3P)AuCl$ with chlorine occurs cleanly and quantitatively to afford $(Ph_3P)AuCl_3$, the same protocol was extended to attempt the synthesis of $AuCl_3$@PPh_2-PEGPIILS, as this precursor would contain gold(III) impregnated on a phosphine-decorated PIIL, which would then enable a comparative evaluation of the performance of phosphine-stabilized AuNPs generated from Au(I) and Au(III) to be undertaken. Although the reaction between AuCl@PPh_2-PEGIILS and chlorine resulted in complete consumption of the Au(I) precursor, analysis by ^{31}P NMR spectroscopy showed it formed a 2:3 mixture of $AuCl_3$@PPh_2-PEGPIILS and AuCl@O = PPh_2-PEGPIILS and repeat reactions conducted with an excess of chlorine gave a similar ratio of products. Since the generation of AuNPs from such a mixture would not provide meaningful results for a comparative study with its Au(I) counterpart the synthesis of this precursor was not pursued. Future studies will focus on polymer modifications to explore whether the PEG unit and/or the nature of the heteroatom influences this oxidation as well as the use of alternative oxidants such $PhICl_2$.

2.2. Selective Partial Reduction of Nitrobenzene to *N*-Phenylhydroxylamine

The reduction of nitrobenzene was used as the benchmark transformation on the basis that there have been several recent reports of the selective partial reduction of nitrobenzene to *N*-phenylhydroxylamine and we have also recently demonstrated that AuNPs supported by heteroatom donor-modified PIILs are highly efficient and selective catalysts for the partial reduction of nitroarenes to *N*-phenylhydroxylamine in water, azoxyarene in ethanol and aniline after longer reaction times or at elevated temperatures. A preliminary comparison of the efficacy of nanoparticles generated from **3a**–**c** was conducted under the optimum conditions identified in our earlier study to explore the influence of the gold precursor (Au(III)/Au(I)) and the heteroatom donor (PPh_3/O = PPh_3) on catalyst efficiency.[106] Initial reactions were conducted in water under an atmosphere of nitrogen at 25 °C using a 0.05 mol% loading of **4a**–**c** generated in situ by sodium borohydride-mediated reduction of the corresponding precursor AuCl@O = PPh_2-PEGPIILS (**3a**), $AuCl_4$@O = PPh_2-PEGPIILS (**3b**) and AuCl@PPh_2-PEGPIILS (**3c**) with a substrate/$NaBH_4$ ratio of 2.5. Under these conditions, catalyst **4a** generated from gold(I)-impregnated phosphine oxide-decorated PIIL **3a** gave complete conversion after only 60 min to afford *N*-phenylhydroxylamine as the sole product, i.e., with

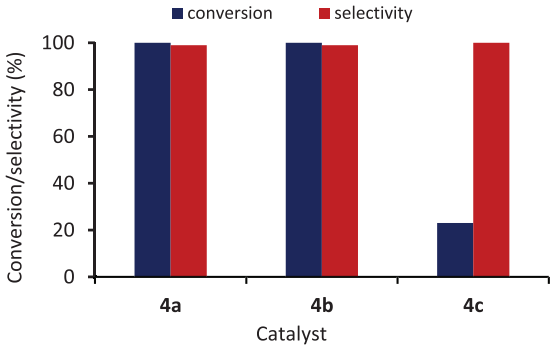

Figure 5. Conversion and selectivity for the sodium borohydride-mediated partial reduction of nitrobenzene to *N*-phenylhydroxylamine under nitrogen in water using catalysts **4a**–**c** generated from 0.05 mol% **3a**–**c**. Each reaction was conducted in triplicate. Reaction conditions: 1 mmol nitrobenzene, 2.5 mmol $NaBH_4$, 0.05 mol% **3a**–**c**, 2 mL water, 25 °C, 60 min. Conversion and selectivity were determined by ^1H NMR spectroscopy using dioxane as internal standard. Selectivity for *N*-phenylhydroxylamine = [% *N*-phenylhydroxylamine/(% *N*-phenylhydroxylamine + % aniline + % azoxybenzene)] × 100.

100% selectivity. Under the same conditions catalyst **4b**, generated by reduction of tetrachloroaurate-impregnated phosphine oxide-decorated PIIL **3b** also gave complete conversion to afford *N*-phenylhydroxylamine with 100% selectivity after the same time; this suggests that the efficacy of the AuNPs does not depend on whether the nanoparticles are generated from a Au(I) or Au(III)-based precursor when immobilized in phosphine oxide-decorated PIIL **2**. Interestingly, and in stark contrast to catalysts generated from precursors **3a** and **3b**, the reduction of nitrobenzene catalyzed by gold nanoparticles generated from Au(I)-impregnated phosphine-modified PIIL **3c** only reached 23% conversion after the same time, albeit with 100% selectivity for *N*-phenylhydroxylamine; the disparate performance between these catalysts is clear from the conversions shown in Figure 5.

The markedly disparate performance between catalysts **4a**–**b** and **4c** prompted us to monitor the progress and composition of the reaction as a function of time to explore the reaction profile and obtain initial turnover frequencies (TOFs) to compare their efficiency against previously reported systems. A series of parallel reductions were conducted in water at 25 °C across a range of reaction times using a 0.05 mol% loading of precatalysts **3a**–**c** and the composition was quantified by ^1H NMR spectroscopy using 1,4-dioxane as an internal standard. The resulting profiles in Figure 6 clearly show that the reaction compositions obtained with catalysts **4a** and **4b** map extremely closely to each other and that both catalysts are markedly more active than **4c**; the former reached initial TOFs of 2280 and 1980 mol nitrobenzene converted mol Au^{-1} h^{-1}, respectively, based on the total metal content, which are substantially higher than the 460 mol nitrobenzene converted mol Au^{-1} h^{-1} obtained with **4c**. While the total metal content is the most common method of reporting the activity of a nanoparticle catalyst, as this approach accounts for the total cost of the catalyst, initial TOFs have also been determined based on the estimated surface metal atoms, as this is more representative of the intrinsic activity of the catalyst. To this end, the difference in activity between **4a**–**b** and

Table 1. Summary of initial TOFs for the sodium borohydride-mediated partial reduction of nitrobenzene to *N*-phenylhydroxylamine catalyzed by **4a–c**.

Catalyst	TOF[a)]	TOF[b)]	TOF[c)]	TOF[d)]
	Mole Nitrobenzene Converted mol Au^{-1} h^{-1}			
4a	2280	8142	2620	9358
4b	1980	5580	2385	6626
4c	460	1069	978	2274

[a)] TOFs based on the total metal loading and determined at ca. 20% conversion.
[b)] TOFs based on the estimated surface metal atoms; full details of the calculations are provided in the Supporting Information.
[c)] TOFs based on the at.% Au(0) calculated from XPS data, full details are provided in Table S10.
[d)] TOFs based on a combination of the at.% Au(0) and the estimated surface metal atoms.

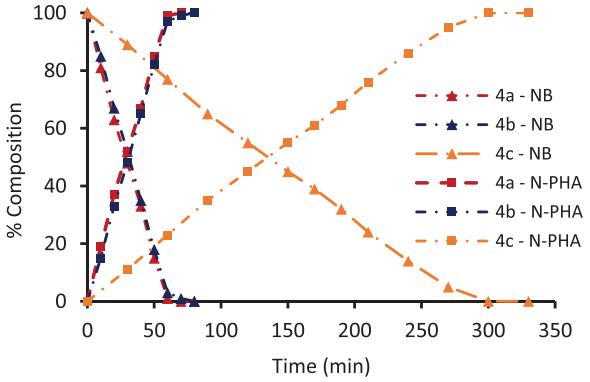

Figure 6. Composition as a function of time for the sodium borohydride-mediated selective partial reduction of nitrobenzene (NB) to *N*-phenylhydroxylamine (*N*-PHA) in water at 25 °C catalyzed by 0.05 mol% **4a** (red), **4b** (blue), and **4c** (orange).

4c is even more evident when the TOFs are calculated using this approach, as shown by the data in Table 1. Finally, as XPS analysis of the catalyst revealed that the ratio of Au(0) to Au(I) species varied quite dramatically as a function of the precatalyst and the reducing agent, TOFs have also been determined based on the at.% of Au(0) species, which were calculated by quantitative analysis of the 4f components in the XPS spectrum. Regardless of whether the TOFs are calculated using the at.% Au(0) or a combination of the at.% Au(0) and the estimated surface metal atoms, catalysts **4a** and **4b** both have markedly higher initial TOFs than **4c**, although the difference in activity is slightly less pronounced for TOFs calculated using the former method; this suggests that the proportion of Au(0) to Au(I) species may contribute to the difference in activity. Moreover, the profiles in Figure 6 also reveal that reductions catalyzed by **4a** and **b** reach complete conversion with >99% selectivity for *N*-phenylhydroxylamine after only 60 min while the corresponding reduction catalyzed by **4c** required 300 min to reach completion, albeit, also with >99% selectivity for *N*-phenylhydroxylamine. The efficacy of **4a** and **b** was further investigated by reducing the catalyst loading to 0.005 mol% and, under otherwise identical conditions, the conversions of 26% and 23%, respectively, with 100% selectivity for *N*-phenylhydroxylamine after 1.5 h correspond to TOFs of 3400 and 3050 mol nitrobenzene converted mol Au^{-1} h^{-1}, respectively. A further reduction in the catalyst loading to 0.0025 mol% did not improve this TOF, which suggests that these turnover numbers probably reflect their potential intrinsic turnover rates.

A comparison of the efficacy of the catalysts generated from **3a–c** with AuNPs generated in the presence of sodium citrate at 80 °C (AuNP@citrate) resulted in a modest conversion of only 44% after 60 min, with a slightly lower selectivity of 89% due to the formation of 1,2-diphenylhydrazine and aniline. The low conversion and initial TOF obtained with AuNP@citrate parallels that recently reported for gold nanoparticle-catalyzed reductions in a comparative study between PEG-terminated polymers and dendritic 1,2,3-triazoles.[121c] Moreover, a $NaBH_4$-mediated reduction of nitrobenzene conducted with AuNPs generated in situ from 0.05 mol% $AuCl_4$@O = PPh_2-PEGPIILS by reduction with an excess of sodium citrate only reached 47% conversion after 60 min to afford *N*-phenylhydroxylamine as the major product in 96% selectivity, together with a minor amount of aniline. The low conversions obtained with AuNPs generated by citrate reduction of $[AuCl_4]^-$ or $AuCl_4$@O = PPh_2PEGPIILS may be due to their size as the average diameters of 14.5 ± 1.9 nm and 10 ± 6.1 nm, respectively, are significantly larger than those for **4a–c** (Figure S36). Furthermore, generation of the AuNPs from $[AuCl_4]^-$-impregnated polymer appears to be crucial to achieving high activity and selectivity as AuNPs generated in aqueous solution in the absence of stabilizer and subsequently stirred with polymer **2** for 10 min prior to addition of nitrobenzene only reached 34% conversion. Thus, it appears that impregnation of the polymer-immobilized ionic liquid with the gold precursor, either in the form of gold(I) or gold(III), is necessary to achieve the highest selectivity, which may indicate that the support influences NP growth although we cannot rule out the influence of surface properties such as sterics and hydrophilicity or even surface-support interactions. The influence of the support on NP growth was confirmed by TEM analysis of the AuNPs generated by borohydride reduction of an aqueous solution of $[AuCl_4]^-$ prior to stirring with O = PPh_2-PEGPIILS as the average diameter of 21.8 ± 5.1 nm is markedly larger than those generated from the gold-impregnated precursor $AuCl_4$@O = PPh_2PGPIILS (**3b**) (Figure S36).

The efficacy of **4a–c** as catalysts for the partial reduction of nitrobenzene to *N*-phenylhydroxylamine was also compared with that of PtNP@PPh_2-PEGPIILS as there have been several reports of efficient and selective reduction of nitrobenzene using platinum nanoparticle-based catalysts, including PtNP@amberlite,[44] platinum nanowires coated with

ethylenediamine,[51] and Pt/C deactivated with either an amine or DMSO.[47,48] Under the conditions described above, 0.05 mol% PtNP@PPh_2-PEGPIILS catalyzed the sodium borohydride-mediated reduction of nitrobenzene in water at 25 °C to afford 64% conversion with 83% selectivity for *N*-phenylhydroxylamine after 60 min; this low selectivity is due to competing formation of aniline and 1,2-diphenylhydrazine. Control reactions for the reduction of nitrobenzene conducted in water with 2.5 equiv of $NaBH_4$ after replacing the pre-catalysts with polymers **1** or **2** gave negligible conversion even after 2 h, confirming that the AuNPs were essential for catalysis.

Although any comparison of the performance of **4a–c** as catalysts for the partial reduction of nitrobenzene to *N*-phenylhydroxylamine against related literature reports must be treated with caution due to the disparate conditions and protocols employed to collect data, the different methods and conversions used to calculate TOFs and the absence of detail for the calculations, a comparison of the efficacy of **4a** against these systems revealed that it appears to be amongst the most active. For example, the initial TOF of 2280 mol nitrobenzene converted mol Au^{-1} h^{-1} obtained with 0.05 mol% **4a** at 25° C is higher than the 830 mol nitrobenzene converted mol Ru^{-1} h^{-1} obtained at 25 °C in THF with RuNPs stabilized on carbon nanotubes,[42] 1800 mol nitrobenzene converted mol Pt^{-1} h^{-1} obtained in methanol at 25 °C with ethylenediamine-coated ultrathin platinum nanowires,[51] 900 mol nitrobenzene converted mol Pd^{-1} h^{-1} with palladium nanoclusters in water–ethanol at 25 °C[50] and a substantial improvement on the 234 mol nitrobenzene converted mol Ru^{-1} h^{-1} at room temperature in chloroform with polystyrene-supported RuNPs,[43] 61 mol nitrobenzene converted mol Pt^{-1} h^{-1} obtained with PtNP@amberlite IRA 900 in PEG-450 at 60 °C,[44] 87 mol nitrobenzene converted mol Ir^{-1} h^{-1} with polystyrene-supported IrNPs in PEG-400 at 85 °C,[46] and 200 mol nitrobenzene converted mol Pt^{-1} h^{-1} for 5 wt% Pt/SiO_2 with an amine additive[47] but lower than the 13,940 mol nitrobenzene converted mol Pt^{-1} h^{-1} reported for NanoSelect nanoparticulate platinum solid catalyst supported on activated carbon,[45] and 8760 mol nitrobenzene converted mol Ru^{-1} h^{-1} with RuNP stabilized by phosphine oxide-decorated PIIL (see Table S3 in the Supporting Information).[112] It is worth noting that several of the *N*-phenylhydroxylamine selective nanoparticle-based systems described above required the use of an organic solvent such as chloroform or THF to achieve high selectivity and/or needed a high catalyst loading, a high reaction temperature or a long reaction time whereas **4a** and **4b** gave near quantitative conversion with high selectivity for *N*-phenylhydroxylamine in short reactions times and with high TOFs in water under mild conditions; this is a significant improvement on existing protocols and as such may well be a practical and viable system for use in greener synthesis and scale-up.

In several cases, high selectivity for the nanoparticle-catalyzed partial reduction of nitrobenzene has been attributed to differential adsorption of the nitrobenzene and *N*-phenylhydroxylamine at the surface of the nanoparticle. For instance, the electron-rich surface of ethylenediamine-modified platinum nanoparticles favors adsorption of the electron-deficient nitrobenzene substrate but disfavors adsorption of the electron-rich *N*-phenylhydroxylamine such that the latter readily dissociates from the surface before it can be further reduced. While the high selectivity obtained with AuNP@PPh_2-PEGPIILS (**4c**) may be attributed to a similar interfacial electronic effect modulating the adsorption energies by donation of electron density from the phosphine to the surface of the nanoparticle, it is not clear that the high selectivities associated with **4a** and **4b** are due to such an effect as phosphine oxides are poor donors and are more likely to act as hemilabile modifiers. In this case, the high selectivity associated with **4a** and **4b** may be due to the hydrophilic environment created by the polar PEG and phosphine oxide which could influence the relative binding affinity of the nitrobenzene and *N*-phenylhydroxylamine and/or their activation. While **4a–c** are all highly selective for the partial reduction of nitrobenzene to *N*-phenylhydroxylamine, **4a** and **4b** are markedly more active than **4c**. Interestingly, the key difference between **4a**, **4b** and **4c** is that the former are supported on a PIIL decorated with a hemi-labile phosphine oxide while the latter is stabilized by a triarylphosphine-modified PIIL. Thus, this marked difference in activity could be associated with the nature of the heteroatom as electron donation from a tertiary phosphine would render the surface electron-rich and disfavor hydride transfer such that it may become rate limiting. In contrast, the phosphine oxide in **4a** and **4b** may facilitate hydride transfer from the borohydride to afford an active surface Au-H species, possibly via a cooperative process involving a hydrogen-bonded ensemble between a surface-coordinated borohydride, water protons and the oxygen atom of the hemilabile phosphine oxide, such as that shown in Figure 7(i). Moreover, a hydrogen bond between the protonated P═O and an oxygen atom of a surface-coordinated nitrobenzene (or a hydrogen-bonded ensemble involving the phosphine oxide, the hydrogen atoms of water and the oxygen atom of nitrobenzene) could also active the nitrobenzene and facilitate the hydride transfer step (Figure 7(iii)). Alternatively, the large excess of phosphine donor relative to the number of surface metal atoms may saturate the active sites and hinder access of the substrate whereas the phosphine oxide could act as a hemilabile donor and readily dissociate from the surface to facilitate substrate binding. To this end, further polymer modifications are currently underway to explore which components influence activity and selectivity while surface electronic effects will be probed by CO stripping voltammetry and DFT calculations and mechanistic studies involving kinetic isotope effects and in operando surface investigations will be undertaken to develop a better understanding of the role of the phosphine oxide in this reduction and thereby inform the design of more efficient catalysts.

2.3. Selective Partial Reduction of Nitrobenzene to Azoxybenzene

As our initial disclosure reported a solvent-dependent selectivity profile for the partial reduction of nitrobenzene catalyzed by **4a** that gave quantitative conversion to *N*-phenylhydroxylamine

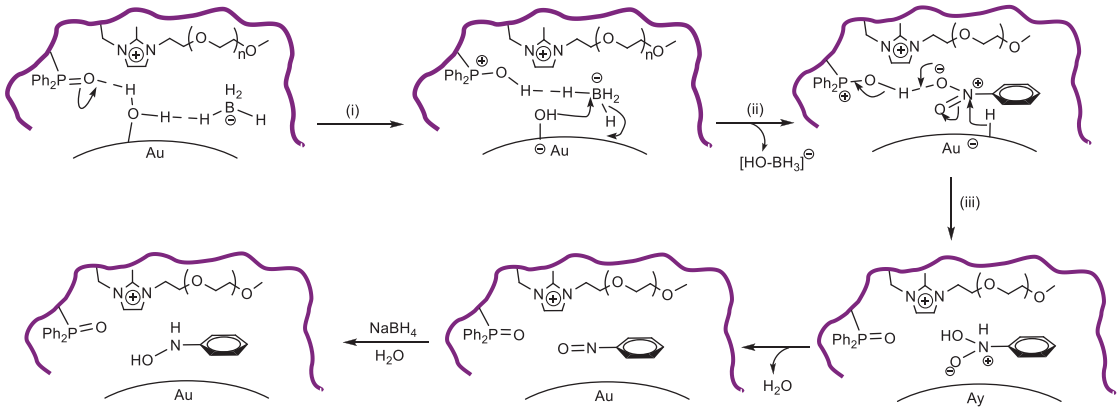

Figure 7. Possible pathway for the $NaBH_4$-mediated partial reduction of nitrobenzene to *N*-phenylhydroxylamine catalyzed by **4a** and **b**.

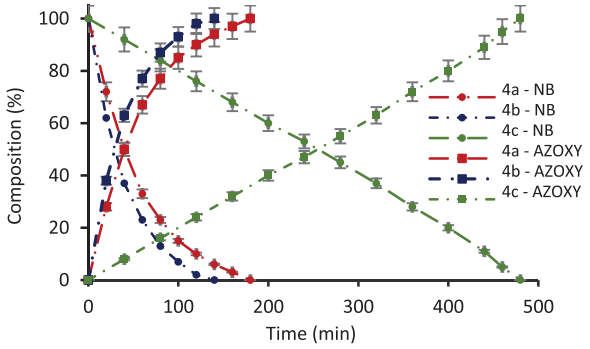

Figure 8. Reaction profile as a function of time for the selective partial reduction of nitrobenzene (NB) to azoxybenzene (AZOXY) in ethanol at 25 °C using 2.5 equiv of $NaBH_4$ and catalyzed by 0.05 mol% **4a** (red), **4b** (blue), and **4c** (green).

when the reduction was conducted in water and complete conversion to azoxybenzene in ethanol, the composition of the partial reduction of nitrobenzene to azoxybenzene in ethanol catalyzed by 0.05 mol% **4a–c** was monitored as a function of time to compare the reaction profiles for each of the catalysts, details of which are presented in Figure 8. The resulting profile for catalyst **4a**, obtained by analyzing a series of parallel reductions conducted across a range of reaction times, shows that azoxybenzene forms cleanly as the only observable product with an initial TOF of 1680 h^{-1} and that 100% conversion with complete selectivity for azoxybenzene was obtained after 3 h. However, when the reaction time was extended to 4 h the selectivity decreased due to formation of azobenzene, diphenylhydrazine, and aniline, which is indicative of reduction via the condensation pathway.[129] Interestingly, the corresponding composition-time profile for the same partial reduction using 0.05 mol% **4b** revealed that this catalyst is slightly more active than **4a** as the reduction reached 77% conversion after only 60 min with an initial TOF of 2220 h^{-1}. While **4c** also catalyzed the partial reduction of nitrobenzene to afford azoxybenzene with high selectivity it was much less active than either **4a** or **4b** with an initial TOF of 240 h^{-1}; moreover, the reduction only reached 23% conversion after 2 h and ultimately required 8 h to reach complete conversion, albeit also with 100% selectivity for azoxybenzene. Background reactions for the reduction of nitrobenzene in ethanol conducted under identical conditions but substituting **3a–c** with 0.05 mol% **1** and **2** gave negligible conversion (<2%) after the same time (3 h), which confirms catalysis by AuNPs. The parallels between the performance profiles of **4a, 4b** and **4c** in water and ethanol suggest that the same factors may be responsible for the similarity in their selectivity for *N*-phenylhydroxylamine and azoxybenzene, respectively, and the disparity in their activity; we suggested above that the former may well be associated with selective adsorption due to the hydrophilic environment at the surface while the latter may well be due to the different influence of the phosphine and phosphine oxide on the surface electronic properties which modulates the hydride transfer kinetics such that hydride transfer to the electron-rich surface in **4c** may be slow and possibly rate limiting.

A survey of the literature revealed that there are relatively few examples of the selective partial reduction of nitrobenzene to azoxybenzene with nanoparticle-based catalysts and a comparison of their efficacy against that for **4b** revealed it to be amongst the most active and selective to be reported. For example, the TOF of 2220 h^{-1} is markedly higher than the 60 h^{-1} obtained with gold nanoparticles supported on mesostructured ceria (AuNP@CeO_2), a switchable solvent selective catalyst that gave azoxybenzene using 2-propanol as the hydrogen donor and azobenzene in a 1:1 mixture or 2-propanol and water.[130] Other recent examples of NPs that catalyze the selective reduction of nitrobenzene to azoxybenzene with a lower TOF than **4b** include iridium-based hierarchically coiled ultrathin nanosheets doped with *N*-butylamine which gave an initial TOF of 400 h^{-1}, albeit with only 89% selectivity for azoxybenzene,[131] magnetically separable Ni/graphene nanocomposites which gave azoxybenzene as the sole product but with a TOF of only 16.8 h^{-1},[132] single atom ruthenium coordinated to the oxygen atoms in CeO_2 (Ru-SAs/CeO_2) which gave 78% selectivity for azoxybenzene at 65% conversion,[133] bifunctional NiNPs covered by a few layers of carbon and CeO_2 nanoparticles (Ni@C-CeO_2) which only reached 35% conversion after 150 min at 120 °C but with 95% selectivity for azoxybenzene,[134] bimetallic PdCuNPs which achieved a TOF of 40 h^{-1} with 89.9% selectivity for azoxybenzene,[135] gold clusters and Au single atoms on layered double hydroxides combined with *closo*-dodecaborate with an optimum TOF

of 125 h^{-1} to azoxybenzene with 97% selectivity,[136] visible light induced photocatalytic reduction with ZrO_2-supported Ag–Cu alloy nanoparticles which gave azoxy compounds with modest selectivities but with TOFs in the order of 2.0 h^{-1},[137] and a bismuth porphyrin MOF which was highly selective for the light-promoted reduction of nitroarenes to the corresponding azoxyarene, azoarene and hydrazoarene with TOFs up to 250 h^{-1}.[138] The initial TOF of 2220 h^{-1} for **4b** is also comparable to the 1960 h^{-1} obtained at 20 °C with zirconium phosphate-supported AgNPs[139] but lower than the 6750 h^{-1} for in situ-generated ultrasmall palladium nanoclusters which catalyzed the tandem reduction of a range of nitroarenes to the corresponding *N*-arylhydroxylamine which were subsequently oxidized to the corresponding azoxyarene,[50] as well as 40,377 h^{-1} for the solvent-free hydrogenation of nitrobenzene catalyzed by Co single atoms decorated on Nb_2O_5 nanomeshes (see Table S4 in the Supporting Information).[140]

2.4. Complete Reduction of Nitrobenzene to Aniline

Finally, as there are a host of gold nanoparticle-based systems that catalyze the complete reduction of nitrobenzene to the corresponding aniline,[141–143] a study with catalyst **4a–c** was undertaken to identify optimum conditions for the complete reduction of nitrobenzene to aniline to compare their efficacy against existing catalysts. Using the protocol described above, the reduction of nitrobenzene was monitored as a function of time in water at 60 °C using catalyst generated in situ from 0.05 mol% **3a–c** to compare the reaction profiles and rates for each catalyst. The composition-time profiles associated with **4a** and **4b** are qualitatively similar (Figure 9a,b) and show that the nitrobenzene is rapidly consumed in the early stages of the reaction reaching ca. 90% conversion after only 20 min with concomitant formation of *N*-phenylhydroxylamine as the major species (ca. 80–85%) together with a minor amount of aniline (ca. 10–15%) as the only other identifiable product; not surprisingly, the initial TOF of 9600 and 7680 mol nitrobenzene converted Au^{-1} h^{-1} for **4a** and **4b**, respectively, are comparable to each other and markedly higher than those determined at 25 °C. Longer reaction times resulted in steady consumption of the *N*-phenylhydroxylamine and the generation of increasing amounts of aniline, which was eventually obtained as the sole product in quantitative yield after 180 min. In stark contrast, the corresponding composition-time profile for the reduction of nitrobenzene with catalyst **4c** revealed it to be markedly more sluggish as the reaction occurred over a much longer timescale with an initial TOF of 1360 mol nitrobenzene converted Au^{-1} h^{-1}, albeit with a qualitatively similar composition profile to those catalyzed by **4a** and **4b**. For example, although complete conversion of the nitrobenzene required ca. 3–4 h, the maximum selectivity of 88% for *N*-phenylhydroxylamine after 2 h is comparable to the 84% and 85% obtained with catalysts **4a** and **4b**, respectively, after 20 min; moreover, as for the reductions catalyzed by **4a** and **4b**, aniline was the only other identifiable product. The composition-time profiles in Figure 9a–c indicate that the reduction occurs via the direct pathway as there is no evidence for azoxy-based

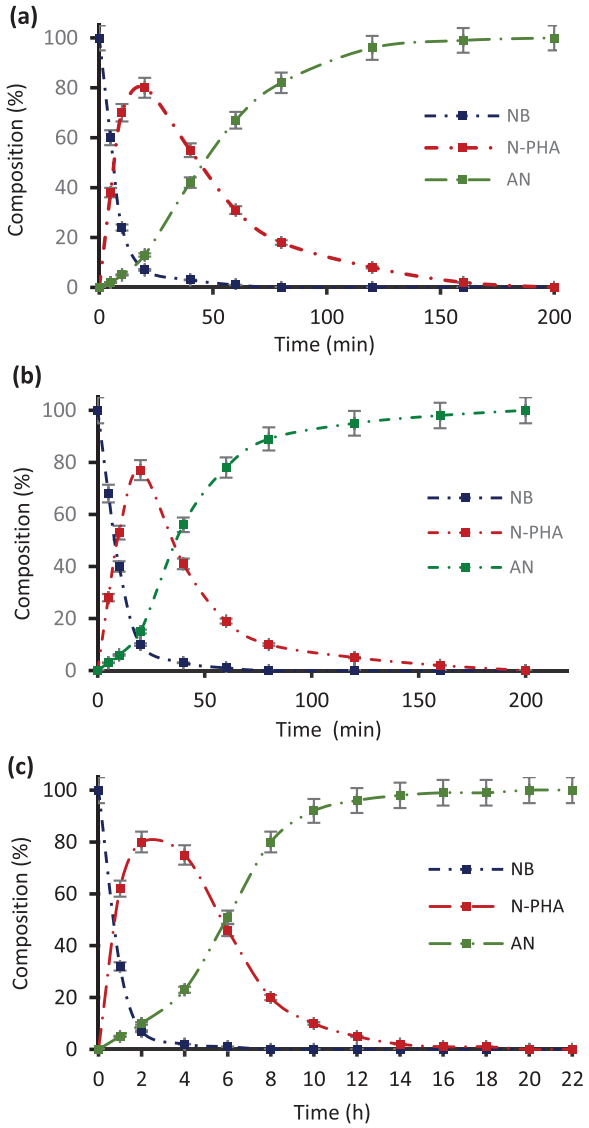

Figure 9. Composition profiles as a function of time for the $NaBH_4$-mediated reduction of nitrobenzene (NB) to aniline (AN) via *N*-phenylhydroxylamine (*N*-PHA) at 60 °C in water catalyzed by 0.05 mol% (a) **4a**, (b) **4b** and (c) **4c**.

species. A similar profile has recently been reported for the Ru(II) catalyzed reduction of nitrobenzene to aniline which also gave *N*-phenylhydroxylamine as the only observable intermediate,[144] whereas the corresponding reduction with gold nanoparticles stabilized by imidazolium-based porous organic polymers formed *N*-phenylhydroxylamine, azoxybenzene and hydrazobenzene en route to aniline.[145] When the loading of **4a** was reduced to 0.005 mol%, complete reduction to aniline was reached after only 22 h at 60 °C, which corresponds to a TON of 20,000 with an initial TOF of 11,700 mol nitrobenzene converted Au^{-1} h^{-1}, as measured by the conversion of 29% after 30 min. A comparison of the efficiency of **4a** against some recent examples of the AuNP-catalyzed reduction of nitroarenes revealed that the initial TOF of 9600 h^{-1} obtained in water with 0.05 mol% **4a** is significantly higher than 33 h^{-1} for mesostructured ceria-supported gold nanoparticles,[130] 27 h^{-1} with gold nanoparticles deposited

on nanocrystalline magnesium oxide,[146] 400 h^{-1} obtained in water with hybrid gold nanoparticle-reduced graphene oxide nanosheets,[147] 167 h^{-1} for *Aspergillus trinidadensis*-supported gold nanoparticles,[148] 107 h^{-1} using gold nanoparticles supported on NiO and CuO,[149] 240 h^{-1} obtained with gold nanoparticles stabilized on starch functionalized creatine,[150] 83 h^{-1} with gold nanoparticles anchored on magnetic poly(ionic-liquid),[151] 83 h^{-1} for gold nanoparticles supported on ionic liquid-modified cellulose,[152] 1230 h^{-1} for AuNPs confined in a nanoporous polymer matrix,[153] 960 h^{-1} for gold nanoparticles supported by imidazolium-based porous organic polymers,[144] 333 h^{-1} with water-soluble gold nanoparticles stabilized by a nitrogen-rich poly(ethyleneglycol)-tagged substrate,[154] 405 h^{-1} obtained with Au/TiO_2,[155,156] 1976 h^{-1} achieved with MoS_2/nitrogen doped graphene decorated with gold nanoparticles,[157] and 6 12 h^{-1} for self-assembled amine-functionalized gold nanoparticles on phosphonate-functionalized graphene nanosheets[158] and even higher than the 8798 h^{-1} reported for ultra small gold nanoparticles stabilized on SBA-15 functionalized *N,N,N*-pincer ligand.[159]

2.5. Marked Enhancement in Activity for the Partial Reduction of Nitrobenzene to *N*-Phenylhydroxylamine Using DMAB as the Hydrogen Donor

While our preliminary disclosure of the selective partial reduction of nitrobenzene to *N*-phenylhydroxylamine reported the use of sodium borohydride as the hydrogen donor, the kinetics of this multi-step reduction are clearly complicated as the selectivity and yields for *N*-phenylhydroxylamine appear to depend on the combination of metal nanoparticle/support as well as the hydrogen donor and the solvent. To this end, there are several catalyst systems in which hydrazine hydrate has been reported to be the hydrogen donor of choice to achieve high selectivity and yields for the reduction of nitrobenzene to *N*-phenylhydroxylamine; examples include RuNP supported on carbon nanotubes in THF,[42] RuNP@polystyrene in THF or chloroform,[43] RuNP on polymer-immobilized ionic liquid in ethanol,[112] IrNP@polystyene in PEG-400[46] and PtNP@amberlite in PEG-400.[44] The high selectivities obtained with these systems prompted us to investigate the efficacy of **4a**–**c** as catalysts for the reduction of nitrobenzene using hydrazine hydrate as the hydrogen donor. Interestingly, negligible conversions were obtained in water or ethanol even after 2 h at 25 °C using catalyst generated from 0.05 mol% **3a**–**c** and 2.5 equiv of hydrazine hydrate. Similarly, formic acid triethylamine azeotrope was also an ineffective hydrogen donor under these conditions, i.e., the selectivity for partial reduction of nitroarenes is clearly dependent on the combination of metal nanoparticle and hydrogen donor. Surprisingly though, complete conversion and > 99% selectivity for *N*-phenylhydroxylamine was obtained in water at room temperature after only 10 min using 2.5 equiv of dimethylamine borane (DMAB) as the hydrogen donor and a 0.05 mol% loading of precatalyst **3a**; this represents a marked and substantial enhancement in activity compared with the corresponding $NaBH_4$-mediated reduction which required 60 min to reach complete conversion. The disparate performance of **4a** as a catalyst for the partial reduction of nitrobenzene with these hydrogen donors is most evident from a comparison of the initial TOFs of 15,600 mol nitrobenzene converted mol Au^{-1} h^{-1} and 2280 mol nitrobenzene converted mol Au^{-1} h^{-1} with DMAB and $NaBH_4$, respectively. Similarly, **4b** also exhibited a comparable improvement in activity when DMAB was used as the donor and gave quantitative conversion to afford *N*-phenylhydroxylamine as the sole product after only 8 min with an initial TOF of 20,400 mol nitrobenzene converted mol Au^{-1} h^{-1} compared with 1980 mol nitrobenzene converted mol Au^{-1} h^{-1} under the same conditions with $NaBH_4$. Even though **4c** is much less active than either **4a** or **4b** as a catalyst for the $NaBH_4$-mediated partial and complete reduction of nitrobenzene, its activity also improved quite dramatically when DMAB was used as the hydrogen donor as complete conversion to *N*-phenylhydroxylamine with 99% selectivity was achieved after only 100 min; although this is significantly longer than the 8–10 min reaction time required for catalysts **4a** and **4b**, it is much shorter than the 480 min needed to reach complete conversion with $NaBH_4$. Moreover, the initial TOF of 1560 mol nitrobenzene converted mol Au^{-1} h^{-1} is also a marked improvement on the corresponding TOF of 460 mol nitrobenzene converted mol Au^{-1} h^{-1} for the $NaBH_4$-mediated reduction. Background reductions of nitrobenzene conducted under the same conditions but replacing precatalysts **3a** and **3b** with 0.05 mol% **1** or **2** gave ca. 5% conversion to azoxybenzene and *N*-phenylhydroxylamine confirming that AuNPs are required to achieve high activity and selectivity.

Even when the TOFs for the DMAB-mediated reductions are calculated by accounting for the estimated percentage of surface metal atoms, the at.% Au(0) or a combination of both as described above, **4a** and **4b** are both markedly more active than **4c**, although the difference in the initial TOFs is not as marked for those based on the at.% Au(0) as was found for the $NaBH_4$-mediated reduction. A comparison of the composition profile mapped as a function of time for **4a** and **4b** with **4c** in Figure 10a,b emphasizes the disparate performance between these catalysts as well as the enhancement in their efficacy compared with the use of $NaBH_4$ as the hydrogen donor (Figure 6). Such high TOFs obtained with **4a** and **4b** in water under mild conditions are unprecedented for the DMAB-mediated partial reduction of nitroarenes and future studies will aim to exploit their high activity by integration of the catalyst into a continuous flow packed bed reactor to assess their suitability for scale-up production of active pharmaceutical ingredients.

TEM analysis of **4a**–**c** generated in situ by reduction with DMAB as the hydrogen donor for the partial reduction of nitrobenzene revealed that the nanoparticles were essentially monodisperse and that those for **4a** (3.3 ± 1.6 nm), **4b** (3.1 ± 1.3 nm) and **4c** (2.6 ± 0.8 nm), were all similar in size. Representative micrographs of **4a**–**c** generated by reduction of **3a**–**c** with DMAB and the corresponding distribution histograms based on sizing of >100 nanoparticles are shown in Figure 11 and Figures S25, S29, and S33 in the Supporting Information. Interestingly, the nanoparticles generated by reduction of **3a**–**c** with DMAB are comparable in size to those generated with $NaBH_4$ which may indicate that the markedly disparate hydrogen donor-dependent activity of these catalysts is not a function

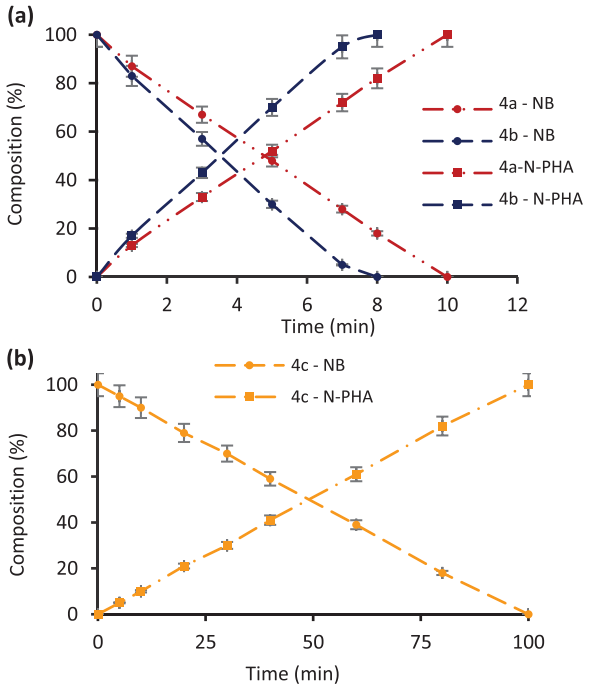

Figure 10. Composition–time profile for the partial reduction of nitrobenzene (NB) to *N*-phenylhydroxylamine (*N*-PHA) conducted under nitrogen in water at 25 °C with 2.5 mol equiv of DMAB using catalysts generated from 0.05 mol% (a) **4a** and **4b** and (b) **4c**.

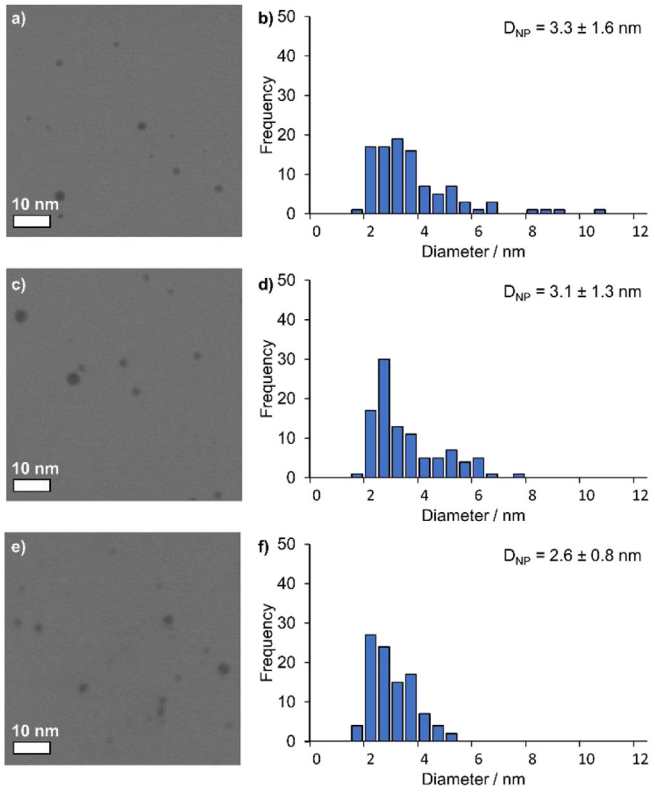

Figure 11. (a, c, and e) HRTEM images of **4a**–**c**, respectively, generated by in situ reduction of **3a**–**c** with dimethylamine borane, and (b, d, and f) corresponding size distribution determined by counting >100 particles. Mean particle diameters are 3.3 ± 1.6, 3.1 ± 1.3, and 2.6 ± 0.8 nm for **4a**, **4b**, and **4c**, respectively. Scale bars are 10 nm (white).

of the size but an intrinsic property of the donor. To this end, further studies will be undertaken to try and identify the origin of this marked difference in efficacy. This will involve the ex situ preparation of AuNP@O = PPh_2PEGPIILS with $NaBH_4$ and DMAB to conduct detailed kinetic studies on the transfer hydrogenation of nitrobenzene as a function of the hydrogen donor coupled with surface investigations as well as a comparison of the AuNP-catalyzed hydrolytic dehydrogenation of $NaBH_4$ and DMAB as this may affect the availability of hydride species at the NP surface.

Interested in determining the scope of this enhancement in activity for the reduction of nitrobenzene using DMAB as the hydrogen donor, its use for the partial reduction of nitrobenzene to azoxybenzene in ethanol was also explored. A series of reactions were conducted under the conditions described above with DMAB to map the composition as a function of time and the resulting data for catalysts **4a** and **4b** (Figure 12a,b) revealed some surprising differences to the corresponding $NaBH_4$-mediated reduction in ethanol. Firstly, the reaction is markedly slower and required 6 h for the nitrobenzene to be completely consumed and, secondly, there is a significant build-up of *N*-phenylhydroxylamine in the early stages of the reaction such that it is the major species after 5 h (ca. 80%), with only minor amounts of azoxybenzene (8%) and aniline (11%). Longer reaction times resulted in gradual consumption of the *N*-phenylhydroxylamine to afford a mixture of aniline and azobenzene, but this conversion was extremely sluggish as evidenced by the composition after 24 h which comprised *N*-phenylhydroxylamine (10%), azoxybenzene (42%) and aniline (48%). Thus, in stark contrast to the DMAB-mediated reduction in water, which experienced a marked enhancement in rate compared to the corresponding reduction with $NaBH_4$ and gave quantitative yields of *N*-phenylhydroxylamine after only 10 min, the DMAB-mediated reduction in ethanol was much slower than its $NaBH_4$-based counterpart and was much less selective for azoxybenzene due to competing reduction to aniline. Catalyst **4c** gave a similar composition-time profile for the DMAB-mediated reduction in ethanol although the consumption of nitrobenzene was significantly slower and occurred over a much longer timescale and required ca. 40 h to reach complete conversion to afford *N*-phenylhydroxylamine as the major species. Longer reaction times resulted in the gradual consumption of the N-phenylhydroxylamine over ca. 110 h to afford a mixture of azoxybenzene (40%) and aniline (55%), with only a trace amount of *N*-phenylhydroxylamine (5%) remaining (Figure 12c). Such a dramatic dependence of the rate and selectivity on the combination of solvent and reducing agent was unexpected, and as such, kinetic measurements, DFT calculations, and in operando FT-IR spectroscopic studies[156,160] will be combined to establish a more detailed understanding of how these factors impact catalyst activity and selectivity.

3. Conclusion

Gold nanoparticles stabilized by phosphine oxide-decorated PIILs (AuNP@O = PPh_2-PEGPIILS) are highly active catalysts for

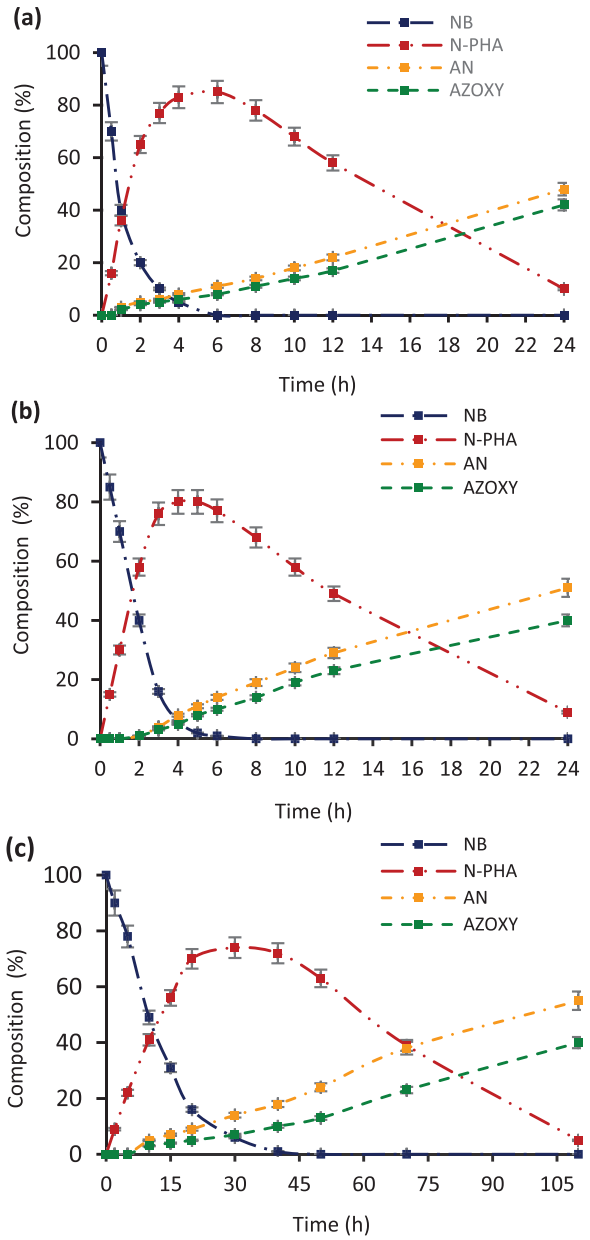

Figure 12. Composition–time profile for the partial reduction of nitrobenzene (NB) to *N*-phenylhydroxylamine (*N*-PHA) and subsequent reduction to azoxybenzene (AZOXY) and aniline (AN) conducted under nitrogen in ethanol at 25 °C with 2.5 mol equiv of DMAB and catalyzed by 0.05 mol% (a) **4a** and (b) **4b**.

the sodium borohydride-mediated partial reduction of nitrobenzene and exhibit a marked solvent-dependent selectivity generating *N*-phenylhydroxylamine as the sole product in water and giving quantitative conversion to azoxybenzene in ethanol. In stark contrast, gold nanoparticles with a similar size and stabilized by phosphine-decorated PIIL, i.e., AuNP@PPh_2-PEGPIILS, are much less active but retain the same selectivity profile. At this stage we can only speculate about the origin of such disparate activities and tentatively suggest that the heteroatom phosphine donor could saturate the surface and prevent access of the substrate and reagents to the active sites or an interfacial electronic effect induced by the phosphine could modify the surface electronic properties and thereby influence the rate of hydride transfer to the surface of the nanoparticle. Surprisingly, the use of dimethylamine borane as the hydrogen donor under otherwise identical conditions resulted in a substantial and marked enhancement in activity for the partial reduction of nitrobenzene to *N*-phenylhydroxylamine and the unoptimized TOF of 20,400 h^{-1} is the highest to be reported for the DMAB-mediated reduction of nitrobenzene to *N*-PHA with a gold nanoparticle-based catalyst. Such high activities in water and under mild conditions should enable greener environmentally benign protocols to be developed. To this end, further catalyst modifications, kinetic measurements on ex situ-generated catalysts as a function of the hydrogen donor and in operando FT-IR investigations are currently underway to develop an understanding of the factors responsible for the extreme hydrogen-donor-dependent activity profiles and to identify a catalyst suitable for integration into a continuous flow packed-bed reactor for the scale-up production of *N*-arylhydroxylamines and aryl amines.[161]

4. Experimental Section

Synthesis of O = PPh_2-PEGPIIL (2): An oven-dried Schlenk flask was allowed to cool to room temperature under vacuum, backfilled with nitrogen, and charged with PPh_2-PEGPIIL (**1**) (1.50 g, 1.00 mmol), dichloromethane (50 mL) and H_2O_2 (35% w/w, 1.70 mL, 15.0 mmol) dissolved in water (2 mL) and the resulting mixture stirred vigorously overnight at room temperature. The organic layer was separated, dried over $MgSO_4$, filtered and the solvent was removed under reduced pressure to afford O = PPh_2-PEGPIIL (**2**) as a white free-flowing powder (1.40 g, 90%). ^{31}P NMR (162 MHz, $CDCl_3$, δ): 29.26; FT-IR (neat, cm^{-1}, $\breve{\upsilon}$): 3340, 2921, 2861, 1911, 1585, 1529, 1511, 1436, 1420, 1400, 1355, 1300, 1257, 1185, 1113, 1093, 1027, 1001, 946, 820, 756, 722, 703, 673, 531.

Synthesis of AuCl@O = PPh_2-PEGPIILS (3a): An oven-dried Schlenk flask was allowed to cool under N_2 and charged with PPh_2-PEGPIIL (**1**) (2.50 g, 1.66 mmol), $KAuCl_4$ (0.63 g, 1.66 mmol) and water (40 mL). The reaction mixture was stirred overnight at room temperature. The solvent was removed under reduced pressure, and the resulting residue was dissolved in dichloromethane (10 mL/g polymer) and added dropwise to a large volume of diethyl ether (350 mL) and stirred for 60 min. After this time, the mixture was allowed to settle and the product was filtered through a frit, washed with water (2 × 10 mL), ethanol (2 × 10 mL) and diethyl ether (2 × 30 mL) to give AuCl@O = PPh_2-PEGPIIL (**3a**) as an orange powder (2.20 g, 80%). ^{31}P NMR (202 MHz, $CDCl_3$, δ): 29.4; FT-IR (neat, cm^{-1}): $\breve{\upsilon}$ = 3355, 2871, 1585, 1513., 1437, 1349, 1250, 1185, 1093, 943, 830, 752, 722, 704, 539. ICP-OES data: 8.61 wt% gold corresponding to a gold loading of 0.43 mmol g^{-1}.

Synthesis of $AuCl_4$@O = PPh_2-PEGPIILS (3b): According to an adapted literature procedure,[106] an oven-dried Schlenk flask under N_2 was charged with O = PPh_2-PEGPIIL (**2**) (1.18 g, 0.78 mmol), $KAuCl_4$ (0.29 g, 0.78 mmol) and water (25 mL). The reaction mixture was stirred overnight at room temperature. The solvent was removed under reduced pressure and the resulting residue was dissolved in dichloromethane (10 mL/g polymer), added dropwise to a large volume of diethyl ether (350 mL), and stirred for 60 min. After this time, the mixture was allowed to settle and the product

was filtered through a frit, washed with water (2 × 10 mL), ethanol (2 × 10 mL) and diethyl ether (2 × 30 mL) to give $AuCl_4$@O = PPh_2-PEGPIIL (**3b**) as an orange powder (1.10 g, 92%); ^{31}P NMR (202 MHz, $CDCl_3$, δ): 29.4; FT-IR (neat, cm^{-1}, $\tilde{\nu}$): 3346, 3130, 2871, 1642, 1586, 1514, 1436, 1349, 1250, 1174, 1116, 941, 824, 752, 722, 703, 605, 538. ICP-OES data: 8.15 wt% gold corresponding to a gold loading of 0.41 mmol g^{-1}.

Synthesis of AuCl@PPh$_2$-PEGPIILS (3c): An oven-dried Schlenk flask under N_2 was charged with PPh_2-PEGPIIL (**1**) (2.00 g, 1.33 mmol), (THT)AuCl (0.42 g, 1.33 mmol), water (35 mL), and dichloromethane (10 mL). The reaction mixture was stirred overnight at room temperature. The solvent was removed under reduced pressure, and the resulting residue was dissolved in dichloromethane (10 mL/g polymer), added dropwise to a large volume of diethyl ether (400 mL) and stirred for 60 min. After this time, the product was allowed to settle and filtered through a frit, washed with water (2 × 10 mL), ethanol (2 × 10 mL), and diethyl ether (2 × 30 mL) to give AuCl@PPh_2-PEGPIIL (**3c**) as a white powder (2.00 g, 95%). ^{31}P NMR (202 MHz, $CDCl_3$, δ): 33.5; FT-IR (neat, cm^{-1}, $\tilde{\nu}$): 3353, 2871, 1585, 1514, 1436, 1349, 1184, 1099, 945, 847, 751, 695, 667, 610, 540, 509. ICP-OES data: 8.94 wt% gold corresponding to a gold loading of 0.45 mmol g^{-1}.

General procedure for the selective reduction of nitrobenzene to N-phenyl hydroxylamine: An oven-dried Schlenk flask was allowed to cool under N_2 and charged with catalyst (0.05 mol%, 0.5 µmol) and either $NaBH_4$ or $Me_2NH{\cdot}BH_3$ (2.5 mmol) and then evacuated and backfilled with nitrogen several times. Deionized water (2.5 mL) was added, and the resulting mixture stirred at ca. 500 rpm for 5 min at room temperature. After this time, nitrobenzene (1.0 mmol, 1.0 mmol, 0.103 mL, 0.123 g) was added, and the reaction stirred for the appropriate time at 25 °C. The mixture was then quenched by the addition of water (5 mL), the product quickly extracted with ethyl acetate (2 × 20 mL) and the solvent removed under reduced pressure. The resulting residue was analyzed by ^{1}H NMR spectroscopy using 1,4-dioxane as the internal standard to measure the composition of the starting material and the product and to determine the selectivity and conversion.

General procedure for the selective reduction of nitrobenzene to azoxybenzene: An oven-dried Schlenk flask was cooled under nitrogen and charged with catalyst (0.05 mol%, 0.5 µmol) and $NaBH_4$ or $(CH_3)_2NH{\cdot}BH_3$ (2.5 mmol) and ethanol (2 mL). The mixture was stirred at ca. 500 rpm for 5 min at room temperature after which nitrobenzene (1.0 mmol, 0.103 mL, 0.123 g) was added and the resulting mixture stirred for the appropriate time at 25 °C. After this time, 1,4 dioxane (85 µL, 1.0 mmol) was added as the internal standard and a 0.05 mL aliquot removed and diluted with $CDCl_3$. The resulting solution was analyzed by ^{1}H NMR spectroscopy to determine the composition, selectivity, and conversion.

General procedure for the selective reduction of nitrobenzene to aniline: An oven-dried Schlenk flask under N_2 was charged with catalyst (0.05 mol% 0.5 µmol) and $NaBH_4$ (5.0 mmol) and deionized water (2 mL) was added immediately, and the mixture stirred at ca. 500 rpm for 5 min at 60 °C. Then nitrobenzene (1.0 mmol, 0.103 mL, 0.123 g) was added, and the mixture was stirred for the appropriate time at 60 °C. After this time, 1,4 dioxane (85 µL, 1.0 mmol) was added as the internal standard and a 0.05 mL aliquot removed and diluted with $CDCl_3$. The resulting solution was analyzed by ^{1}H NMR spectroscopy to determine the composition, selectivity, and conversion.

Supporting Information

The following files are available free of charge: complete experimental details and general procedures, ^{1}H, ^{13}C, and ^{31}P NMR spectra and TGA trace for polymer support **2**, ^{13}C and ^{31}P NMR spectra, SEM images, and XPS data for precatalysts **3a**–**c**, and SEM and HRTEM images and XPS data for catalysts **4a**–**c** and ^{31}P NMR spectra for the oxidation of PPh_3 with K[$AuCl_4$]. The authors have cited additional references within the Supporting Information.

Acknowledgements

Hussam Y. Alharbi gratefully acknowledges Taibah University, Saudi Arabia, for a scholarship. The authors also thank Dr. Tracey Davey for the SEM images (Faculty of Medical Sciences, Newcastle University) and Zabeada Aslam and the Leeds Electron Microscopy and Spectroscopy Centre (LEMAS) at the University of Leeds for TEM analysis. This research was funded through a studentship (Anthony Griffiths) awarded by the Engineering and Physical Sciences Centre for Doctoral Training in Molecules to Product (EP/SO22473/1). The authors greatly acknowledge their support of this work. UK Catalysis Hub is kindly thanked for resources and support provided via our membership of the UK Catalysis Hub Consortium and funded by EPSRC grants: EP/R026939/1, EP/R026815/1, EP/R026645/1, EP/R027129/1, EP/M013219/1 (biocatalysis). This article is dedicated to the memory of Professor Stephen A. Westcott (Canada Research Chair holder in the Department of Chemistry & Biochemistry, Mount Allison University, Canada), who recently passed away; a fantastic and inspired scientist, a great ambassador for chemistry teaching and research in Canada and across the globe, a selfless, generous, and kind human being, but most of all, a genuine, true, and most sincere friend who is greatly missed.

Conflict of Interests

The authors declare no conflict of interest.

Data Availability Statement

The data that support the findings of this study are available in the Supporting Information of this article.

Keywords: Gold(I) and gold(III)-derived nanoparticles · *N*-Phenylhydroxylamine and azoxybenzene · Partial reduction of nitrobenzene · Phosphine oxide and phosphine-decorated polymer-immobilized ionic liquids · Solvent-dependent selectivity

[1] Z. Rappaport, *The Chemistry of Hydroxylamines, Oximes and Hydroxamic Acids*, Wiley, Chichester, West Sussex, **2009**.
[2] W. Uhl, A. Kyriatsoulis, *Namen and Schlagwortreaktionen in der Organischen Chemie*, Vieweg & Teubner Verlag, Wiesbaden, **1984**.

[3] P. M. Vyas, S. Roychowdhury, P. M. Woster, C. K. Svensson, *Biochem. Pharmacol.* **2005**, *70*, 275–286.
[4] J. S. Yadav, B. V. S. Reddy, P. Streedhar, *Adv. Synth. Catal.* **2003**, *345*, 564–567.
[5] C. K. Svensson, *Chem. Res. Toxicol.* **2003**, *16*, 1035–1043.
[6] D. K. Nio, K. Zhao, *J. Am. Chem. Soc.* **1999**, *121*, 2456–2459.
[7] M. G. Kallitsakis, D. I. Ioannou, M. A. Terzidis, G. E. Kostakis, I. N. Lykakis, *Org. Lett.* **2020**, *22*, 4339–4343.
[8] P. Kumar, *Pharmacology and Therapeutics for Dentistry*, 7th ed., Elsevier, St Loius, MO **2017**, 457–487.
[9] Y. Qu, J. C. Spain, *Environ. Microbiol.* **2011**, *13*, 1010–1017.
[10] R. Singh, U. Manjunatha, H. I. Boshoff, Y. H. Ha, P. Niyomrattanakit, R. Ledwidge, C. S. Dowd, I. Y. Lee, P. Kim, L. Zhang, S. Kang, T. H. Keller, J. Jiricek, C. W. Barry, *Science* **2008**, *322*, 1392–1395.
[11] M. D. Corbett, B. R. Chipko, *Antimicrob. Agents Chemother.* **1978**, *13*, 193–198.
[12] K. Shudo, T. Okamoto, *Tetrahedron Lett.* **1973**, *21*, 1839–1842.
[13] K. Shudo, T. Ohta, T. Okamoto, *J. Am. Chem. Soc.* **1981**, *103*, 645–653.
[14] H. Takeuchi, J.-I. Tateiwa, S. Hata, K. Tsutsumi, Y. Osaki, *Eur. J. Org. Chem.* **2003**, 3920–3922.
[15] A. D. McGill, W. Zhang, J. Wittbrodt, J. Wang, H. B. Schlegel, P. G. Wang, *Biorg. Med. Chem.* **2000**, *8*, 405–412.
[16] A. T. Balaban, R. E. Garfield, M. J. Lesko, W. A. Seitz, *Org. Prep. Proceed. Int.* **1998**, *30*, 439–446.
[17] J. D. Spence, A. E. Raymond, D. E. Norton, *Tetrahedron Lett.* **2003**, *44*, 849–851.
[18] F. Ahmad, J. B. Hughes, *Environ. Sci. Technol.* **2002**, *36*, 4370–4381.
[19] C.-M. Ho, T.-C. Lau, *New J. Chem.* **2000**, *24*, 859–863.
[20] R. S. Srivastava, K. M. Nicholas, *J. Am. Chem. Soc.* **1997**, *119*, 3302–3310.
[21] R. N. Ram, V. K. Soni, *J. Org. Chem.* **2013**, *78*, 11935–11947.
[22] E. Bamberger, *Ber. Dtch. Chem. Ges. Chem.* **1894**, *27*, 1548–1557.
[23] Y. A. Wang, L. W. Ye, L. M. Zhang, *Chem. Commun.* **2011**, *47*, 7815–7817.
[24] R. B. Harris, I. B. Wilson, *Tetrahedron Lett.* **1983**, *24*, 231–232.
[25] C. Kashima, N. Yoshiwara, Y. Omote, *Tetrahedron Lett.* **1982**, *23*, 2955–2956.
[26] L. A. Carpino, C. A. Giza, B. A. Carpino, *J. Am. Chem. Soc.* **1959**, *81*. 955–957.
[27] D. Beaudoin, J. D., Wuest, *Tetrahedron Lett.* **2011**, *52*, 2221–2223.
[28] H. Feuer, B. F. Vincent, Jr., R. S. Bartlett, *J. Org. Chem.* **1965**, *30*, 2877–2880.
[29] H. Feuer, R. S. Bartlett, B. F. Vincent, Jr., R. S. Anderson, *J. Org. Chem.* **1965**, *30*, 2880–2882.
[30] P. D. Ren, X. W. Pan, Q. H. Jin, Z. P. Yao, *Synth. Commun.* **1997**, *27*, 3497–3503.
[31] K. Yanada, H. Yamaguchi, H. Meguri, S. Uchida, *J. Chem. Soc. Chem. Commun.* **1986**, 1655–1656.
[32] M. S. Mourad, R. S. Varma, G. W. Kabalka, *J. Org. Chem.* **1985**, *50*, 133–135.
[33] H. Feuer, B. F. Vincent, *J. Am. Chem. Soc.* **1962**, *84*, 3771–3772.
[34] For a recent review of the catalytic reduction of nitro compounds to phenylhydroxylamine and its derivatives see: a) M. Yu, D. Ouyang, L. Wang, Y.-N. Liu, *Molecules* **2024**, *29*, 4353; b) P. Ren, T. Dong, S. Wu, *Synth. Commun.* **1997**, *27*, 1547–1552.
[35] S. Q. Xun, L. R. Wen, J. Kun, Z. Z. Xi, Z. De Feng, *Chem. Lett.* **2006**, *35*, 226–227.
[36] S. Ung, A. Falguières, A. Guy, C. Ferroud, *Tetrahedron Lett.* **2005**, *46*, 5913–5917.
[37] M. Bartra, P. Romea, F. Urpí, J. Vilarrasa, *Tetrahedron* **1990**, *46*, 587–594.
[38] S. Liu, Y. Wang, J. Jiang, Z. Jin, *Green Chem.* **2009**, *11*, 1397–1400.
[39] I. D. Entwistle, T. Gilkerson, R. A. W. Johnstone, R. P. Telford, *Tetrahedron* **1978**, *34*, 213–215.
[40] P. W. Oxley, B. M. Adger, M. J. Sasse, M. A. Forth, *Org. Synth.* **1989**, *67*, 187–192.
[41] L. Pernoud, J. P. Candy, B. Didillon, R. Jacquot, J. M. Basset, *Stud. Surf. Sci. Catal.* **2000**, *130*, 2057–2062.
[42] D. V. Jawale, E. Gravel, C. Boudet, N. Shah, V. Geertsen, H. Li, I. N. N. Namboothiri, E. Doris, *Chem. Commun.* **2015**, *51*, 1739–1742.
[43] J. H. Tyler, S. H. Nazari, R. H. Patterson, V. Udumula, S. J. Smith, *Tetrahedron Lett.* **2017**, *58*, 82–86.
[44] A. K. Shila, P. Das, *Green Chem.* **2013**, *15*, 3421–3428.
[45] E. H. Boymans, P. T. Witte, D. Vogt, *Catal. Sci. Technol.* **2015**, *5*, 176–183.
[46] D. Bhattacherjee, Shaifali, A. K., G. V. Zyryanov, P. Das, *Mol. Catal.* **2021**, *514*, 111836.
[47] Y. Takenaka, T. Kiyosu, J. C. Choi, T. Sakakura, H. Yasuda, *Green Chem.* **2009**, *11*, 1385–1390.
[48] S. L. Karwa, R. A. Rajadhyaksha, *Ind. Eng. Chem. Soc.* **1987**, *26*, 1746–1750.
[49] Y. Takenaka, T. Kiyosu, G., Mori, J.-C. Choi, T. Sakakura, H., Yasuda, *Catal. Today* **2011**, *164*, 580–584.
[50] Z. Yan, X. Xie, Q. Song, F. Ma, X. Sui, Z. Huo, M. Ma, *Green Chem.* **2020**, *22*, 1301–1307.
[51] G. Chen, C. Xu, X. Huang, J. Ye, L. Gu, G. Li, Z. Tang, B. Wu, H. Yang, Z. Zho, Z. Zhou, G. Fu, N. Zheng, *Nature Mat.* **2016**, *15*, 564–569.
[52] D. Li, G. Lu, C. Cai, *Catal. Commun.* **2020**, *137*, 105949.
[53] L. Lu, Z. Zou, B. Fang, *ACS Catal.* **2021**, *11*, 6020–6058.
[54] K. Liu, R. Qin, N. Zheng, *J. Am. Chem. Soc.* **2021**, *143*, 4483–4499.
[55] For an insightful account on metal nanoparticles immobilized on molecularly modified surfaces for controlled hydrogenation and hydrogenolysis see:A. Bordet, W. Leitner, *Acc. Chem. Res.* **2021**, *54*, 2144–2157.
[56] L. M. Rossi, J. L. Fiorio, M. A. S. Garcia, C. P. Ferraz, *Dalton Trans.* **2018**, *47*, 5889–5915.
[57] S. Campisi, M. Schiavoni, C. E. Chan-Thaw, A. Villa, *Catalysts* **2016**, *6*, 185.
[58] X. Wang, Y.-F. Jiang, Y.-N. Liu, A.-W. Xu, *New J. Chem.* **2018**, *42*, 19901–19907.
[59] M. Sankar, Q. He, R. V. Engel, M. A. Sainna, A. J. Logsdail, A. Roldan, D. J. Willock, N. Agarwal, C. J. Kiely, G. J. Hutchings, *Chem. Rev.* **2020**, *120*, 3890–3938.
[60] S. Jayakumar, A. Modak, M. Guo, H. Li, X. Hu, Q. Yang, *Chem. Eur. J.* **2017**, *23*, 7791–7797.
[61] Z. Wang, H. Jiang, *RSC Adv.* **2015**, *5*, 34622–34629.
[62] H. Jiang, X. Zheng, *Catal. Sci. Technol.* **2015**, *5*, 3728–3734.
[63] J. L. Castlebou, E. Bresó-Femenia, P. Blondeau, B. Chaudret, S. Castillón, C. Claver, G. Cyril, *ChemCatChem* **2014**, *6*, 3160–3168.
[64] M. Ibrahim, M. A. S. Garcia, L. L. R. Vono, M. Guerrero, P. Lecante, L. M. Rossi, K. Philippot, *Dalton Trans.* **2016**, *45*, 17782–17791.
[65] Y. Lei, Z. Chen, G. Lan, R. Wang, X.-Y. Zhou, *New J. Chem.* **2020**, *44*, 3681–3689.
[66] G. D. Kalita, P. Sarmah, P. K. Saikia, L. Saikia, P. Das, *New J. Chem.* **2019**, *43*, 4253–4260.
[67] L. Wu, Z.-W. Li, F. Zhang, Y.-M. He, Q.-H. Fan, *Adv. Synth. Catal.* **2008**, *350*, 846–862.
[68] I. Cano, A. M. Chapman, A. Urakawa, P. W. M. N. van Leeuwen, *J. Am. Chem. Soc.* **2014**, *136*, 2520–2528.
[69] N. Almora-Barrios, I. Cano, P. W. M. N. van Leeuwen, N. Lopez, *ACS Catal.* **2017**, *7*, 3949–3954.
[70] I. Cano, M. A. Huertos, A. M. Chapman, G. Buntkowsky, T. Gutmann, P. B. Groszewicz, P. W. M. N. van Leeuwen, *J. Am. Chem. Soc.* **2015**, *37*, 7718–7727.
[71] M. Guo, H. Li, Y. Ren, X. Ren, Q. Yang, C., Li, *ACS Catal.* **2018**, *8*, 6476–6485.
[72] X. Ren, M. Guo, H. Li, C. Li, L. Yu, J. Liu, Q. Yang, *Angew. Chem., Int. Ed.* **2019**, *58*, 14483–14488.
[73] S. G. Kwon, G. Krylova, A. Sumer, M. M. Schwartz, E. E. Bunel, C. L. Marshall, S. Chattopadhyay, B. Lee, J. Jellinek, E. V. Shevchenko, *Nano Lett.* **2012**, *12*, 5382–5388.
[74] W. Long, N. A. Brunelli, S. A. Didas, E. W. Ping, C. W. Jones, *ACS Catal.* **2013**, *3*, 1700–1708.
[75] F. P. da Silva, J. L. Fiorio, L. M. Rossi, *ACS Omega* **2017**, *2*, 6014–6022.
[76] Z. Guo, C. Xiao, R. V. Maligal-Ganesh, L. Zhou, T. W. Goh, X. Li, D. Tesfagaber, A. Thiel, W. Huang, *ACS Catal.* **2014**, *4*, 1340–1348.
[77] I. Schrader, J. Warneke, J. Backenköhler, S. Kunz, *J. Am. Chem. Soc.* **2015**, *137*, 905–912.
[78] H. Liu, Q. Mei, S. Li, Y. Yang, Y. Y. Wang, H. Liu, L. R. Zheng, P. An, J. Zhang, B. Han, *Chem. Commun.* **2018**, *54*, 908–911.
[79] M. R. Axet, S. Conejero, I. C. Gerber, *ACS Appl. Nano. Mater.* **2018**, *1*, 5885–5894.
[80] M. Guo, C. Li, Q. Yang, *Catal. Sci. Technol.* **2017**, *7*, 2221–2227.
[81] B. Wu, H. Huang, J. Yang, N. Zheng, G. Fu, *Angew. Chem., Int. Ed.* **2012**, *51*, 3440–3443.
[82] S. Rana, S. B., Jonnalagadda, *RSC Adv.* **2017**, *7*, 2869–2879.
[83] Z. Tian, D.-L. Chen, T. He, P. Yang, F.-F. Wang, Y. Zhong, W. Zhu, *J. Phys. Chem. C* **2019**, *123*, 22114–22122.

[84] D. Chandra, S. Saini, S. Bhattacharya, A. Bhaumik, K. Kamata, M. Hara, *ACS Appl. Mater. Interfaces* **2020**, *12*, 52668–52677.
[85] S. Masuda, K. Mori, Y. Futamura, H. Yamashita, *ACS Catal.* **2018**, *8*, 2277–2285.
[86] K. Mori, S. Masuda, H. Tanaka, K. Yoshizawa, M. Chee, H. Yamashita, *Chem. Commun.* **2017**, *53*, 4677–4690.
[87] H. Zhong, M. Iguchi, M. Chatterjee, T. Ishizaka, M. Kitta, Q. Xu, H. Kawanami, *ACS Catal.* **2018**, *8*, 5355–5362.
[88] V. Srivastava, *Catal. Lett.* **2021**, *151*, 3704–3720.
[89] Q. Liu, X. Yang, L. Li, S. Miao, Y. Li, Y. Li, X. Wang, Y. Huang, T. Zhang, *Nature Commun.* **2017**, *8*, 1407.
[90] J. B. Ernst, C. Schwermann, G. Yokota, M. Tada, S. Muratsugu, N. L. Doltsinis, F. Glorius, *J. Am. Chem. Soc.* **2017**, *139*, 9144–9147.
[91] J. B. Ernst, S. Muratsugu, F. Wang, M. Tada, F. Glorius, *J. Am. Chem. Soc.* **2016**, *138*, 10718–10721.
[92] L. M. Martínez-Prieto, A. Ferry, L. Rakers, C. Richter, P. Lecante, K. Philippot, B. Chaudret, F. Glorius, *Chem. Commun.* **2016**, *52*, 4768–4771.
[93] C. Richter, K. Schaepe, F. Glorius, B. J. Ravoo, *Chem. Commun.* **2014**, *50*, 3204–3207.
[94] P. Lara, L. M. Martínez-Prieto, M. Roselló-Merino, C. Richter, F. Glorius, S. Conejero, K. Philippot, B. Chaudret, *Nano-Struct. Nano-Obj.* **2016**, *6*, 39–45.
[95] A. Rühling, K. Schaepe, L. Rakers, B. Vonhören, P. Tegeder, B. J. Ravoo, F. Glorius, *Angew. Chem., Int. Ed.* **2016**, *55*, 5856–5860.
[96] A. Ferry, K. Schaepe, P. Tegeder, C. Richter, K. M. Chepiga, B. J. Ravoo, F. Glorius, *ACS Catal.* **2015**, *5*, 5414–5420.
[97] A. M. Ruiz-Varilla, E. A. Baquero, B. Chaudret, E. de Jesus, C. Gonzalez-Arellano, J. C. Flores, *Catal. Sci. Technol.* **2020**, *10*, 2874–2881.
[98] Z. Cao, D. Kim, D. Hong, Y. Yu, J. Xu, S. Lin, X. Wen, E. M. Nichols, K. Jeong, J. A. Reimer, P. Yang, C. J. Chang, *J. Am. Chem. Soc.* **2016**, *138*, 8120–8125.
[99] L. Zhang, Z. Wei, S. Thanneeru, M. Meng, M. Kruzyk, G. Ung, B. Liu, J. He, *Angew. Chem., Int. Ed.* **2019**, *58*, 15834–15840.
[100] Z. Cao, J. S. Derrick, J. Xu, R. Gao, M. Gong, E. M. Nichols, P. T. Smith, X. Liu, X. Wen, C. Copéret, C. J. Chang, *Angew. Chem., Int. Ed.* **2018**, *57*, 4981–4985.
[101] Z. Cao, Z. S. B. Zacate, X. Sun, J. Liu, E. M. Hale, W. P. Carson, S. B. Tyndall, J. Xu, X. Liu, X. Liu, C. Song, J.-H. Luo, M.-J. Cheng, X. Wen, W. Liu, *Angew. Chem., Int. Ed.* **2018**, *57*, 12675–12679.
[102] M. Khavani, A. Mehranfar, M. R. K. Mofrad, *J. Phys. Chem. B* **2022**, *126*, 9617–9631.
[103] S. Doherty, J. G. Knight, T. Backhouse, E. Abood, H. Al-shaikh, A. R. Clemmet, J. R. Ellison, R. A. Bourne, T. W. Chamberlain, R. Stones, N. J. Warren, I. J. S. Fairlamb, K. R. J. Lovelock, *Adv. Synth. Catal.* **2018**, *360*, 3716–3731.
[104] S. Doherty, J. G. Knight, T. Backhouse, E. Abood, H. Al-shaikh, I. J. S. Fairlamb, R. A. Bourne, T. W. Chamberlain, R. Stones, *Green Chem.* **2017**, *19*, 1635–1641.
[105] S. Doherty, J. G. Knight, T. Backhouse, A. Bradford, F. Saunders, R. A. Bourne, T. W. Chamberlain, R. Stones, A. Clayton, K. R. J. Lovelock, *Catal. Sci. Technol.* **2018**, *8*, 1454–1467.
[106] S. Doherty, J. G. Knight, T. Backhouse, R. J. Summers, E. Abood, W. Simpson, W., Paget, R. A. Bourne, T. W. Chamberlain, R. Stones, K. R. J. Lovelock, J. M. Seymour, M. A. Isaacs, C. Hardacre, H. Daly, N. H. Rees, *ACS Catal.* **2019**, *9*, 4777–4791.
[107] S. Doherty, J. G. Knight, T. Backhouse, T. S. T. Tran, R. Paterson, F. Stahl, H. Y. Alharbi, T. W. Chamberlain, R. A. Bourne, R. Stones, A. Griffiths, J. P. White, Z. Aslam, C. Hardacre, H. Daly, J. Hart, R. H. Temperton, J. N. O'Shea, N. H. Rees, *Catal. Sci. Technol.* **2022**, *12*, 3549–3567.
[108] S. Doherty, J. G. Knight, H. Y. Alharbi, R. Paterson, C. Wills, C. Dixon, L. Šiller, T. W. Chamberlain, A. Griffiths, S. M. Collins, K. Wu, M. D. Simmons, R. A. Bourne, K. R. J. Lovelock, J. M. Seymour, *ChemCatChem* **2022**, e202101752.
[109] S. Doherty, J. G. Knight, R. Paterson, A. Alharbi, C. Wills, C. Dixon, L. Šiller, T. W. Chamberlain, A. Griffiths, S. M. Collins, K.-J. Wu, M. D. Simmons, R. A. Bourne, K. R. J. Lovelock, J. Seymour, *Mol. Catal.* **2022**, *528*, 112476.
[110] R. Paterson, L. E. Fahy, E. Arca, C. Dixon, C. Wills, H. Yan, A. Griffiths, S. M. Collins, K. Wu, R. A. Bourne, T. W. Chamberlain, J. G. Knight, S. Doherty, *Chem. Commun.* **2023**, *59*, 12370–13473.
[111] S. Doherty, J. G. Knight, A. A. Alharbi, C. Wills, T. W. Chamberlain, R. A. Bourne, A. Griffiths, S. M. Collins, K.-J. Wu, M. D. Simmons, *ChemCatChem* **2023**, *15*, e202300418.
[112] S. Doherty, J. G. Knight, R. Paterson, C. Wills, T. W. Chamberlain, A. Griffiths, S. M. Collins, K.-J. Wu, M. D. Simmons, *J. Catal.* **2023**, *417*, 74–88.
[113] For a recent insightful review, describing the use of covalently supported ionic liquids in catalysis see: a) F. Giacalone, M. Gruttadauria, *ChemCatChem* **2016**, *8*, 664–684; b) K. Manojkumar, A. Sivaramakrishna, K. Vijayakrishna, *J. Nanoparticle Res.* **2016**, *18*, 103.
[114] K. L. Luska, P. Migowskia, W. Leitner, *Green Chem.* **2015**, *17*, 3195–3206.
[115] a) C. Amatore, A. Jutand, M. A. M'Barki, *Organometallics* **1992**, *11*, 3009–3013; b) C. Amatore, E. Carrie, A. Jutand, M. A. M'Barki, *Organometallics* **1995**, *14*, 1818–1826; c) B. P. Fors, P. Krattiger, E. Strieter, S. L. Buchwald, *Org. Lett.* **2008**, *10*, 3505–3508.
[116] H. Ohmori, S. Nakai, M. Masui, *J. Chem. Soc. Perkin Trans. 1* **1978**, 1333–1335.
[117] W. J. Ramsay, N. A. Bell, Y. Qing, H. Bayley, *J. Am. Chem. Soc.* **2018**, *140*, 17538–17546.
[118] D. J. Gorin, B. D. Sherry, F. D. Toste, *Triphenylphosphinegold(I) Chloride, Encyclopedia of Reagents for Organic Synthesis*, Wiley online library **2008**, https://doi.org/10.1002/047084289X.
[119] N. Mézailles, L. Ricard, F. Gagosz, *Org. Lett.* **2005**, *7*, 4133–4136.
[120] a) G. Biagiotti, V.i. Langè, C. Ligi, S. Caporali, M. Muniz-Miranda, A. Flis, K. M. Pietrusiewicz, G. Ghini, A. Brandi, S. Cicchi, *Beilstein J. Nanotechnol.* **2017**, *8*, 485–493; b) W. E. Swartz Jr., J. K. Ruff, D. M. Hercules, *J. Am. Chem. Soc.* **1972**, *94*, 5227–5229; c) P. Gobbo, W. Luo, S. Ju Cho, X. Wang, M. C. Biesinger, R. H. E. Hudsona, M. S. Workentin, *Org. Biomol. Chem.* **2015**, *13*, 4605–4612; d) F. Kang, X. Qu, P. J. J. Alvarez, D. Zhu, *Environ. Sci. Technol.* **2017**, *51*, 2776–2785; e) W. Wang, A. Zheng, P. Zhao, C. Xia, F. Li, *ACS Catal.* **2014**, *4*, 321–327; f) H. Xu, K. Zhou, J. Si, C. Li, G. Luo, *Catal. Sci. Technol.* **2016**, *6*, 1357–1366; g) G. Lanza, M. J. Martinez Jimenez, F. Alvarez, J. A. Perez-Taborda, A. Avila, *ACS Omega* **2022**, *7*, 34521–34527; h) J.-P. Sylvestre, S. Poulin, A. V. Kabashin, E. Sacher, M. Meunier, J. H. T. Luong, *J. Phys. Chem. B* **2004**, *108*, 16864–16869; i) J. Luo, X. Luo, M. Xie, H.-Z. Li, H. Duan, H.-G. Zhou, R.-J. Wei, G.-H. Ning, D. Li, *Nature Commun.* **2022**, *13*, 7771; j) K. Zhou, J. Jia, C. Li, H. Xu, J. Zhou, G. Luo, F. Wei, *Green Chem.* **2015**, *17*, 356–364; k) J.-P. Sylvestrea, A. V. Kabashina, E. Sachera, M., Meuniera, J. H. T. Luong, Proceedings of SPIE - The International Society for Optical Engineering, July **2004**; l) https://sites.cardiff.ac.uk/xpsaccess/reference/gold/; m) https://www.harwellxps.guru/knowledgebase/gold/.
[121] a) N. Li, M. Echeverría, S. Moya, J. Ruiz, D. Astruc, *Inorg. Chem.* **2014**, *53*, 6954–6961; b) C. Wang, L. Salmon, Q. Li, M. E. Igartua, S. Moya, R. Ciganda, J. Ruiz, D. Astruc, *Inorg. Chem.* **2016**, *55*, 6776–6780; c) R. Ciganda, N. Li, C. Deraedt, S. Gatard, P. Zhao, L. Salmon, R. Hernández, J. Ruiza, D. Astruc, *Chem. Commun.* **2014**, *50*, 10126–10129.
[122] Y. Gong, H. Zhong, W. Liu, B. Zhang, S. Hu, R. Wang, *ACS Appl. Mater. Interfaces* **2018**, *10*, 776–786.
[123] a) S. Montolio, C. Vicent, V. Aseyev, I. Alfonso, M. I. Burguete, H. Tenhu, E. García-Verdugo, S. V. Luis, *ACS Catal.* **2016**, *6*, 7230–7237; b) J. Restrepo, R. Porcar, P. Lozano, M. I. Burguete, E. García-Verdugo, S. V. Luis, *ACS Catal.* **2015**, *5*, 4743–4750.
[124] L. Luza, C. P. Rambor, A. Gual, J. A. Fernandes, D. Eberhardt, J. Dupont, *ACS Catal.* **2017**, *7*, 2791–2799.
[125] S. Thawarkar, B. Thombare, N. D. Khupse, *New J. Chem.* **2017**, *41*, 12989–12995.
[126] R. Appel, *Angew. Chem., Int. Ed.* **1975**, *14*, 801–811.
[127] H. Kawai, W. J. Wolf, A. G. DiPasquale, M. S. Winston, F. D. Toste, *J. Am. Chem. Soc.* **2016**, *138*, 587–593.
[128] X. Cai, J. Nie, G. Yang, F. Wang, C. Ma, C. Lu, Z. Chen, *Mater. Lett.* **2019**, *240*, 80–83.
[129] a) E. A. Gelder, S. D. Jackson, C. M. Lok, *Chem. Commun.* **2005**, 522–524; b) A. Corma, P. Concepción, P. Serna, *Angew. Chem., Int. Ed.* **2007**, *46*, 7266–7269; c) F. Haber, *Z. Elektrochem.* **1898**, *22*, 506.
[130] X. Liu, S. Ye, H.-Q. Li, Y.-M. Liu, Y. Cao, K.-N. Fan, *Catal. Sci. Technol.* **2013**, *3*, 3200–3206.
[131] Z.-P. Zhang, X.-Y. Wang, K. Yuan, W. Zhu, T. Zhang, Y.-H. Wang, J. Ke, X.-Y. Zheng, C.-H. Yan, Y.-W. Zhang, *Nanoscale* **2016**, *8*, 15744–15752.
[132] a) M. N. Pahalagedara, L. R. Pahalagedara, J. He, R. Miao, B. Gottlieb, D. Rathnayake, S. L. Suib, *J. Catal.* **2016**, *336*, 41–48; b) C. L. Daniels, D.-J.

Liu, M. A. S. Adamson, M. Knobeloch, J. Vel, *J. Phys. Chem. C* **2021**, *125*, 24440–24450.
[133] B. Wu, T. Lin, R. Yang, M. Huang, H. Zhang, J. Li, F. Sun, F. Song, Z. Jiang, L. Zhong, Y. Sun, *Green Chem.* **2021**, *23*, 4753–4761.
[134] L. Liu, P. Concepción, A. Corma, *J. Catal.* **2019**, *369*, 312–323.
[135] J. Xiang, H. Jin, F. Ju, Y. Lu, F. Wang, *Russ. J. Phys. Chem. A* **2023**, *97*, 1239–1244.
[136] X. Deng, S. Xia, H. Zhao, Z. Wang, B. Qi, X. Zhou, H. Zhang, *Chem. Eng. J.* **2023**, *467*, 143540.
[137] Z. Liu, Y. Huang, Q. Xiao, H. Zhu, *Green Chem.* **2016**, *18*, 817–825.
[138] Y. Zhang, W. Yang, S. Wang, H. Shua, X. Li, S. Fan, Y. Feng, *Adv. Synth. Catal.* **2023**, *365*, 2400–2405.
[139] Y. Qin, Y. Jiang, X. Wei, Y. Ma, H. Liao, Q. Peng, S. Dai, Z. Wang, X. Zhao, Z. Hou, *New J. Chem.* **2023**, *47*, 14380–14394.
[140] Z. Li, X. Lu, C. Guo, S. Ji, H. Liu, C. Guo, X. Lu, C. Wang, W. Yan, B. Liu, W. Wu, J. H. Horton, S. Xin, Y. Wang, *Nature Commun.* **2024**, *15*, 3195.
[141] H. K. Kadam, S. G. Tilve, *RSC Adv.* **2015**, *5*, 83391–83407.
[142] T. Aditya, A. Pal, T. Pal, *Chem. Commun.* **2015**, *51*, 9410–9431.
[143] S. Panigrahi, S. Basu, S. Praharaj, S. Pande, S. Jana, A. Pal, S. K. Ghosh, T. Pal, *J. Phys. Chem. C* **2007**, *111*, 4596–4605.
[144] M. E. Uysal, U. Solmaz, H. Arslan, *Appl. Organomet. Chem.* **2023**, *37*, e7107.
[145] Y. Su, X. Li, Y. Wang, H. Zhong, R. Wang, *Dalton Trans.* **2016**, *45*, 16896–16903.
[146] K. Layek, M. L. Kantam, M. Shirai, D. Nishio-Hamane, T. Sasakid, H. Maheswaran, *Green Chem.* **2012**, *4*, 3164–3174.
[147] Y. Choi, H. S. Bae, E. Seo, S. Jang, K. H. Park, B.-S. Kim, *J. Mater. Chem.* **2011**, *21*, 15431–15436.
[148] A. G. Deshmukh, H. B. Rathod, P. N. Patel, *Results Chem.* **2023**, *6*, 101199.
[149] M. Gholinejad, R. Khezri, S. Nayeri, R. Vishnuraj, B. Pullithadathil, *Mol. Catal.* **2022**, *530*, 112601.
[150] M. Gholinejad, N. Dasvarz, M. Shojafar, J. M. Sansano, *Inorg. Chim. Acta* **2019**, *495*, 118965.
[151] F. M. Moghaddam, S. E. Ayati, H. R. Firouzi, S. H. Hosseini, A. Pourjavadi, *Appl. Organomet. Chem.* **2017**, *31*, e3825.
[152] A. Pourjavadi, Z. Habibi, *Appl. Organomet. Chem.* **2017**, *31*, e3783.
[153] A. Noschese, A. Buonerba, P. Canton, S. Milione, C. Capacchione, A. Grassi, *J. Catal.* **2016**, *340*, 30–40.
[154] W. Guo, R. Pleixats, A. Shafir, *Chem. Asian J.* **2015**, *10*, 2437–2443.
[155] P. Serna, A. Corma, *ACS Catal.* **2015**, *5*, 7114–7121.
[156] M. Boronat, P. Concepción, A. Corma, S. González, F. Illas, P. Serna, *J. Am. Chem. Soc.* **2007**, *129*, 16230–16237.
[157] M. R. Nabid, Y. Bide, N. Fereidouni, *Chem. Lett.* **2018**, *47*, 964–967,
[158] X. Gao, G., Xu, Y. Zhao, S. Li, F. Shi, Y. Chen, *RSC Adv.* **2015**, *5*, 88045–88051.
[159] S. H. Hosseini, N. Zohreh, S. Alipour, C. Busuioc, R. Negrea, *Catal. Commun.* **2018**, *108*, 93–97.
[160] D. Combita, P. Concepción, A. Corma, *J. Catal.* **2014**, *311*, 339–349.
[161] M. Yaghmaei, A. E. Lanterna, J. C. Scaiano, *iScience* **2021**, *24*, 103472.

Manuscript received: October 03, 2024
Revised manuscript received: December 05, 2024
Accepted manuscript online: December 09, 2024
Version of record online: December 23, 2024